bioRxiv preprint doi: https://doi.org/10.1101/2021.07.14.452325; this version posted July 14, 2021. The copyright holder for this preprint (which was not certified by peer review) is the author/funder, who has granted bioRxiv a license to display the preprint in perpetuity. It is made available under aCC-BY-NC 4.0 International license.

Spinal ganglia control nociceptive input to the central nervous system

Han Hao[1], Rosmaliza Ramli[2,3], Caixue Wang[1], Chao Liu[4], Shihab Shah[2], Pierce Mullen[2], Varinder Lall[2], Frederick Jones[2], Jicheng Shao[1], Hailin Zhang[1], David B. Jaffe[5], Nikita Gamper[1,2]*, Xiaona Du[1]*

[1]Department of Pharmacology, Hebei Medical University; The Key Laboratory of Neural and Vascular Biology, Ministry of Education, China; The Key Laboratory of New Drug Pharmacology and Toxicology, Hebei Province; Shijiazhuang 050011 China.

[2]Faculty of Biological Sciences, University of Leeds, Leeds LS2 9JT, UK.
[3]School of Dental Sciences, Universiti Sains Malaysia, Kelantan 16150, Malaysia.

[4]Department of Animal care, Hebei Medical University; The Key Laboratory of Experimental Animal, Hebei Province; Shijiazhuang, 050011 China.

[5]Department of Biology, UTSA Neurosciences Institute, University of Texas at San Antonio, San Antonio, Texas, 78249, USA

*Correspondence to: Xiaona Du (du_xiaona@hotmail.com) or Nikita Gamper (n.gamper@leeds.ac.uk)

Author Contributions: N.G. and X.D. designed and directed the study; H.H., R.R., C.W., C.L., S.S., P.M., V.L., F.J., J.S. and N.X. conducted the experiments and analyzed data; D.B.J performed computational modeling; N.G., X.D. and H.H. wrote the paper, assisted by all the coauthors.

Competing Interest Statement: The authors declare no competing interests.

Keywords: Dorsal root ganglion; GABA; GABAergic neuron precursor cell; Pain; Sensory neuron

bioRxiv preprint doi: https://doi.org/10.1101/2021.07.14.452325; this version posted July 14, 2021. The copyright holder for this preprint (which was not certified by peer review) is the author/funder, who has granted bioRxiv a license to display the preprint in perpetuity. It is made available under aCC-BY-NC 4.0 International license.

Abstract

Accumulating observations suggest that peripheral somatosensory ganglia may regulate pain transmission, yet direct evidence is sparse. Here we show that the peripheral afferent nociceptive information undergoes dynamic filtering within dorsal root ganglia (DRG) and suggest that this filtering occurs at the axonal bifurcations (t-junctions). Using simultaneous *in vivo* electrophysiological recordings from the peripheral (spinal nerve) and central (dorsal root) aspects of rodent spinal nerves, ganglionic transplantation of GABAergic progenitor cells, and optogenetics we demonstrate tonic and dynamic filtering of action potentials traveling through the DRG. Filtering induced by focal application of GABA or optogenetic GABA release from the DRG-transplanted GABAergic progenitor cells was specific to nociceptive fibers. Light-sheet imaging and computer modeling demonstrated that, compared to other somatosensory fiber types, nociceptors have shorter stem axons, making somatic control over t-junctional filtering more efficient. Optogenetically-induced GABA release within DRG enhanced filtering and reduced both acute and chronic inflammatory and neuropathic pain *in vivo*. These findings support the potential gating of pain information within the somatosensory system, and suggests new therapeutic approaches for pain relief.

Significance Statement

We show that the ascending somatosensory information undergoes dynamic filtering within the dorsal root ganglia (DRGs). Filtering (i.e. failure of action potentials to propagate through the axonal bifurcation or ‘t-junction’) is predominant in nociceptive nerve fibers and can be scaled up or down by the activity of GABAergic inhibitory system within the ganglia. Thus, spinal ganglion represents an intrinsic filtering device within the peripheral branch of somatosensory system. These findings may identify new strategies for pain relief.

bioRxiv preprint doi: https://doi.org/10.1101/2021.07.14.452325; this version posted July 14, 2021. The copyright holder for this preprint (which was not certified by peer review) is the author/funder, who has granted bioRxiv a license to display the preprint in perpetuity. It is made available under aCC-BY-NC 4.0 International license.

Introduction

Current understanding of the somatosensory information processing largely assumes that peripheral nerves faithfully deliver peripherally-born action potentials to the spinal cord. The first synapse in the dorsal horn of the spinal cord is assumed to be the first major integration point for action potentials generated at the periphery. Such a view is represented by the Gate Control Theory of pain (1) and its subsequent refinements and modifications (2-4). Yet, it has long been recognised that information processing is more efficient the earlier it begins within the sensory pathway (5-7). Nevertheless, the absence of true synaptic connections or interneurons within peripheral somatosensory nerves and ganglia reasonably led researchers to dismiss them as possible information processing sites. Despite this, growing evidence suggests that a degree of crosstalk between the peripheral fibers (8, 9) or sensory neuron somata (10-12) might exist. Indeed, recent work suggests that action potentials propagating from the peripheral nerve endings of nociceptive nerve terminals to the spinal cord can fail (or be 'filtered') at axonal bifurcation points (t-junctions) within the spinal ganglia (13-19). An intrinsic GABAergic signalling system within spinal ganglia was recently identified as a mechanism responsible for ganglionic filtering and, potentially, for a cross-talk between the individual sensory neurons (15). Yet, direct evidence for how ascending information can be modified within spinal ganglia is sparse. Here we aimed to obtain direct *in vivo* evidence for ganglionic filtering mediated by the GABA signalling system and assess if such filtering can be targeted to control pain. Using *in vivo* electrophysiological recordings from the peripheral and central aspects of the rodent spinal nerve, optogenetic manipulations, stem axon morphometry, and biophysical modelling we demonstrate that the spinal ganglion is a *bona fide* processing device controlling and modifying nociceptive signalling into the CNS. These findings support the existence of a 'peripheral gate' in somatosensory system and suggest new ways of how sensory ganglia can be targeted for pain relief.

Results

Action potentials induced by the excitation of peripheral nerve endings are filtered within the DRG. We first developed a method for *in vivo* electrophysiological recording of extracellular spiking activity from both the peripheral and central branches of the L5 spinal nerve of a rat. Spinal nerve (SN), DRG, and dorsal root (DR) nerves were surgically exposed in anesthetized rat (Fig. 1A, B). SN and DR were then individually suspended on fine hook electrodes, while the DRG was exposed to direct drug application. This preparation allows *i)* synchronous measurement of the firing rates in the peripheral and central aspects of the spinal nerve (before and after the DRG); *ii)* sensory stimulation of the hind paw; *iii)* direct application of compounds or light to the DRG.

In our recordings both the SN and DR usually displayed spontaneous firing activity (Fig. 1C-H), consistent with earlier reports (20, 21). Intraplantar injection of algogenic compounds, capsaicin (a TRPV1 agonist; CAP, 10 μM, 50 μl; Fig. 1C, D) or bradykinin (BK, 100 μM, 50 μl; Fig. 1E, F), significantly increased firing frequency in both SN and DR branches of the nerve, consistent with the evoked nociceptive inputs being transmitted from the peripheral nerve towards the spinal cord. Capsaicin injection increased firing rates to 288% and 295% of basal values in SN and DR nerves, respectively; BK injection increased firing rates in SN and DR to 166% and 246%, respectively.

Recent studies suggest there is a GABAergic inhibition at the DRG, in addition to the well-accepted spinal GABAergic inhibitory network (15, 22, 23). We thus tested how exogenous application of GABA to the DRG would affect the propagation of peripherally-induced nociceptive signals through the ganglion. Direct injection of GABA (200 μM, 3 μl) into the DRG significantly reduced capsaicin- or BK-induced firing rates specifically in the DR aspects of the nerve, having no effect on the firing rates in the peripheral branches (Fig. 1C-F). Thus, GABAergic inhibition at the DRG can induce a prominent filtering of the throughput conduction.

bioRxiv preprint doi: https://doi.org/10.1101/2021.07.14.452325; this version posted July 14, 2021. The copyright holder for this preprint (which was not certified by peer review) is the author/funder, who has granted bioRxiv a license to display the preprint in perpetuity. It is made available under aCC-BY-NC 4.0 International license.

Interestingly, application of the $GABA_A$ receptor antagonist, bicuculline (BIC; 200 μM, 3 μl) to the DRG during continuous recording of tonic activity in both SN and DR (in the absence of any peripheral stimulation) significantly increased firing rate in the DR but not in the SN aspect of the nerve (Fig. 1G, H). This finding is consistent with our previous observation that application of BIC via the L5-DRG-implanted cannula *in vivo* induces nocifensive behavior towards the hind paw (15). Thus, BIC is likely to attenuate tonic filtering in nociceptive fibers passing through the DRG.

The interpretation of experiments presented in Fig. 1 could be complicated by the presence of the ventral root. Even though the experiments were conducted on immobile animals under deep anesthesia, the presence of intact motor fibers in the SN allows for execution of the flexor reflex which could contribute to SN activity via the efferent and re-afferent discharge. To account for such an eventuality, we evaluated the effect of ventral root (VR) transection on the spontaneous and evoked activity in SN and DR (Suppl. Fig. 1A). VR transection had no noticeable effect on either the SN or DR spontaneous activity (Suppl. Fig. 1B, C). Capsaicin, GABA (Suppl. Fig. 1D, E) and BIC (Suppl. Fig. 1F, G) produced effects qualitatively identical to these presented in Fig.1: capsaicin increased firing rate in both SN and DR and GABA reduced this induced firing rate in DR but not SN. BIC increased firing rate in DR but not in SN. Interestingly, when GABA was DRG-injected on its own, without noxious stimulation of the paw, it failed to produce a significant effect on firing rate in both the SN and DR (Suppl. Fig. 1H, I). Another important observation from the experiments presented in Fig. 1 and Suppl. Fig. 1 was that firing rates in the SN were consistently higher than in the DR. Importantly, this was also true for preparations with VR transection (summarized in Suppl. Fig. 1J). Together with the fact that BIC consistently increased firing rates in the DR (with or without VR transection) these findings support the hypothesis for tonic filtering at DRG.

While VR transection eliminated the efferent input, it did not eliminate efferent fibers themselves from the spinal nerve, thus, any spurious activity in those fibers could have contributed to the SN activity and may have contributed to higher firing rates in the SN, as compared to DR. In order to eliminate efferent fibers we took advantage of the fact that VR injury causes progressive degeneration of the motoneurons and preganglionic parasympathetic neurons (PPN)(24). Thus, we performed VR transections (Suppl. Methods) and allowed animals to recover; two weeks after VR transections the recordings similar to these shown in Fig. 1 and Suppl. Fig 1 were repeated. The motor and PPN fiber degeneration was confirmed by almost complete loss of their marker, Choline acetyltransferase (ChAT)(24) at two weeks after VR transection (Suppl. Fig. 2A). Despite the removal of efferent fibers, tonic firing rate in the DR was still significantly lower, as compared to SN; GABA still significantly reduced the capsaicin-induced firing rate in DR but not SN, while BIC increased firing rate in DR but not in SN (Suppl. Fig. 2B-E). Thus, under our experimental conditions, motor neuron input had no significant contribution to either spontaneous or to evoked activity in SN or DR.

When we tested the effects of GABA on the capsaicin-induced firing and of BIC on spontaneous activity in SN and DR in female rats (Suppl. Fig. 3) and on male rats anesthetized with different anesthetic (isoflurane; Suppl. Fig. 4), we obtained results qualitatively identical to these shown in Fig. 1 and Suppl. Fig. 1-2. Thus, GABA-mediated modulation of ganglionic filtering is a phenomenon reliably observed under a variety of experimental conditions in animals of either sex.

In order to better understand filtering of specific spikes in the recordings shown in Fig. 1 and Suppl. Fig. 1 we developed a spike-matching method allowing to correlate SN and DR spikes (Fig. 2A; Suppl. Fig. 5A). This method proved accurate (80 – 100 %) in Poisson-generated spike trains up to 100 Hz; the accuracy was inversely proportional to firing frequency (Suppl. Fig. 5B). Spike sorting extracellular SN waveforms using the WaveClus implementation of super-paramagnetic clustering allowed us to isolate distinct spike clusters (units) and match these between SN and DR recordings. To rule out contamination of DR units with synchronized firing of another fibre, we calculated the mean deviation (represented as a z score) of each waveform in the unit from the mean waveform of the unit (Suppl. Fig. 5C). Any spikes originating from another fibre firing in a temporally correlated way should exhibit a different waveform shape and thus be recognised as an outlier (> 3 z score). The large majority of spikes were within a z score of 3 from

bioRxiv preprint doi: https://doi.org/10.1101/2021.07.14.452325; this version posted July 14, 2021. The copyright holder for this preprint (which was not certified by peer review) is the author/funder, who has granted bioRxiv a license to display the preprint in perpetuity. It is made available under aCC-BY-NC 4.0 International license.

the unit means, suggesting our matching protocol identified homogenous and distinct DR firing units.

A representative experiment capturing the firing activity of four distinct units is shown in Fig. 2B-D. Capsaicin-evoked spike units were clearly identifiable, noted by the onset of activity during application of capsaicin (Fig. 2C, D); these were characterized by a larger amplitude on average (CAP-insensitive units: 14.5±1.5 μV; CAP-sensitive units: 19.6±0.9 μV; $p<0.01$). However, capsaicin-sensitive units could not be well distinguished by latency and spike width in this way. The mean drop in spiking units between SN and DR was significantly greater with GABA administration after CAP (Fig. 2E, F). To understand how features of the spike waveform predict spike failure when passing through the t-junction, we performed multiple linear regression analysis of spike width and amplitude. Spike amplitude was a significant predictor of filtering in the dorsal root with a coefficient of 1.908 ($p<0.01$), indicating that larger amplitudes but not width corresponded with a greater probability of failure to propagate to the DR during baseline conditions. During administration of CAP, spike units with smaller widths (coefficient of -23.35, $p<0.001$) and a trend of larger amplitudes (coefficient of 1.29, $p=0.0825$) were more likely to be filtered. We further characterized spike units as either A-fibre or C-type based on conduction velocity (<1.2 m/s; presumably C-type; >1.2 m/s, presumably A-fibers (25)). Interestingly, this revealed that C-type fibres were indeed significantly more filtered during application of GABA (Fig. 2G).

Taken together, data presented in Fig. 1, 2 and Suppl. Fig. 1-5 suggest: *i)* there is a basal activity in the SN and DR even in the absence of peripheral stimulation; *ii)* the firing rates in the SN are higher than these in DR, suggesting 'tonic filtering' of this basal activity at the DRG. *iii)* DRG-applied $GABA_A$ antagonist (BIC) increased basal firing in the DN but not in the SN, possibly suggesting removal of 'tonic' GABAergic inhibition in DRG. *iv)* Noxious stimulation increases firing rate in both aspects of the nerve, either sides of the DRG (SN and DR), but the DRG-applied GABA reduced firing in the DN specifically, thus enhancing GABAergic filtering in the nociceptive fibers. Exogenous GABA did not affect the basal firing rate (either in the SN or DR) indicating that there might be GABA-dependent and GABA-independent filtering mechanisms.

Transplantation of forebrain GABAergic neuron precursors into the adult mouse DRG *in vivo* delivers an analgesic mechanism. To test how GABAergic filtering of nociceptive transmission at the DRG can be exploited *in vivo*, we adopted an approach developed by Basbaum's group, who were able to transplant and functionally integrate into dorsal spinal cord, embryonic GABAergic progenitor cells from the medial ganglionic eminence (MGE). Transplanted MGE cells were able to compensate for the loss of spinal GABAergic inhibitory system observed in neuropathic pain models (26, 27). We transplanted embryonic MGE cells derived from VGAT-ChR2-eYFP into the L4 DRG of WT C57 mice. L4 DRG was chosen in this case as it is the major contributor to the sciatic nerve in mice (28). At four weeks after the DRG injection we observed numerous YFP-positive cells in the DRG sections (Fig. 3A), fluorescent cells were entirely absent in vehicle-injected control animals.

In order to confirm that transplanted MGE cells can function as GABAergic neurons within DRG, we performed patch-clamp recordings from the DRG neurons juxtaposed to the MGE cells (Fig. 3B-D) using 'loosened' whole L4 DRGs from mice pre-injected (4 weeks) with the VGAT-ChR2-eYFP-expressing MGE (see Methods). Stimulation of the ganglion with the 473 nm blue light induced inward currents in 9/9 DRG neurons, which were in close juxtaposition with MGE cells (Fig. 3B-D). These same neurons also responded to perfusion of 200 μM GABA with very similar inward currents. In contrast, DRG neurons from vehicle-injected mice never responded to blue light (0/8 neurons) but these did respond to GABA (Fig. 3C, D). These results suggest that *i)* implanted MGE progenitor cells can survive and maturate to produce GABA-releasing neurons in DRG; *ii)* stimulus-induced release of GABA by resident neurons can induce a response in neighboring neurons.

Next, we tested if optogenetic release of GABA from the implanted MGE cells can alleviate chronic pain. In these experiments a fiber-optic light guide was implanted into the DRG immediately after the MGE cells transplantation (Fig. 3E; Methods). Chronic inflammation with

bioRxiv preprint doi: https://doi.org/10.1101/2021.07.14.452325; this version posted July 14, 2021. The copyright holder for this preprint (which was not certified by peer review) is the author/funder, who has granted bioRxiv a license to display the preprint in perpetuity. It is made available under aCC-BY-NC 4.0 International license.

hind paw injection of complete Freund's adjuvant (CFA, 20 µl) induced significant mechanical and thermal hyperalgesia (Fig. 3F-H). We then performed mechanical (Fig. 3G) or thermal (Fig. 3H) sensitivity tests while stimulating ipsilateral L4 DRG with blue light. Optical stimulation significantly reduced both types of hyperalgesia in MGE-injected mice. Interestingly, starting from the second week after the CFA injection, both mechanical and thermal hyperalgesia in the MGE-implanted mice started to recover even in the absence of optogenetic stimulation and by the 3rd week after the CFA injection blue light stimulation no longer produced any additional analgesic effect (Fig. 3G, H). We hypothesized that a buildup of tonic GABA release from the transplanted MGE cells in DRG could be responsible for the light-stimulation-independent recovery of the CFA-induced hyperalgesia. This hypothesis was corroborated in experiments, similar to the ones presented in Fig. 3G, H, but in which no optogenetic stimulation was used, to avoid inducing any stimulus-induced GABA release (Suppl. Fig. 6A, B). We also utilized a chronic constriction injury (CCI) model of neuropathic pain in similar experiments (Suppl. Fig. 6C, D). In both models hyperalgesia developed in control (vehicle-injected) and MGE-implanted mice. However, the latter group displayed significantly quicker and better recovery. Collectively, these data suggest that DRG-implanted MGE cells can be stimulated to release GABA locally *in vivo* and that such release produces analgesic effect.

Optogenetic release or direct injection of GABA to the DRG enhances filtering of spikes triggered by noxious but not innocuous stimuli. We hypothesized that the analgesic effect of MGE cells transplanted into the DRG is mediated by GABAergic filtering of pro-nociceptive spikes at the DRG. To test this we used an approach similar to that used in Fig. 1 and Suppl. Fig 1-5, but instead of applying GABA, we stimulated L4 DRG with blue laser light (Fig. 4A). Optogenetic DRG stimulation (3 - 4 weeks after MGE transplantation) gave rise to qualitatively very similar effects to these produced by application of GABA. Firing induced by the hind paw injections of capsaicin (10 µM, 20 µl, Fig. 4B, D) or BK (100 µM, 20 µl, Fig. 4C, E) was significantly inhibited by the light stimulation in DR but not SN. The optogenetic suppression of firing in DR was evident immediately upon application of blue light (Fig. 4B, C; lower right panels).

Application of noxious heat (60° C water; Suppl. Fig. 7A, B) and noxious cold (ice; Suppl. Fig. 7C, D) induced a significant increase of firing frequencies in both SN and DR and optogenetic DRG stimulation significantly inhibited firing rates in DR but not in SN aspects of the nerve. We then tested innocuous and noxious mechanical stimulation. Air puffs and subthreshold (4g) von Frey filament stimulation (Suppl. Fig. 7E-H) increased firing in both SN and DR, presumably via the activation of low threshold mechanoreceptors in the skin (29, 30). Interestingly, optogenetic stimulation of DRGs did not significantly affect the firing frequency in either SN or DR in these experiments (Suppl. Fig. 7E-H). Noxious mechanical stimulation of the paw with a blunt glass needle also significantly increased firing frequencies in both SN and DR. But in this case optogenetic stimulation substantially inhibited firing in DR, but not in SN (Suppl. Fig. 7I, J). Thus, it appears that GABAergic filtering in DRG predominantly exists in nociceptive fibers.

Next, we performed a set of experiments, similar to that shown in Suppl. Fig. 7 but in naïve rats and with the direct injection of GABA into the DRG instead of optogenetic stimulation (Suppl. Fig. 8). There was a pattern similar to that observed with optogenetic stimulation of MGE cells in mice. Firing induced by noxious heat (Suppl. Fig. 8A, B) and noxious cold (Suppl. Fig. 8C, D) was selectively inhibited in the DR but not in the SN by the DRG-applied GABA. No significant effects of DRG-applied GABA were seen when firing was induced by innocuous air puffs or subthreshold von Frey hairs (Suppl. Fig. 8E-H). In contrast, firing induced by the noxious needle prick was reduced in the DR but not in the SN (Suppl. Fig. 8I, J). Striking similarity of the effects of exogenous GABA and optogenetic GABA release in DRG strongly suggest that *i)* the GABAergic system controls filtering efficacy of the ganglia; *ii)* the filtering is most efficient in nociceptive fibers and *iii)* such filtering is the most plausible explanation of the analgesic effect of MGE cells transplanted to the DRG; *iv)* GABAergic filtering exists in both rats and mice.

To test this further we performed single-unit recordings (Fig. 5A); firing was induced by a stimulating electrode placed in SN and recordings were made from the mechanically isolated single DR fibers. A-type and C-type fibers were distinguished by the conduction velocity (A fibers >1.2 m/s; C fibers <1.2 m/s (25)). The firing in both fiber types was blocked by 1 µM TTX applied

bioRxiv preprint doi: https://doi.org/10.1101/2021.07.14.452325; this version posted July 14, 2021. The copyright holder for this preprint (which was not certified by peer review) is the author/funder, who has granted bioRxiv a license to display the preprint in perpetuity. It is made available under aCC-BY-NC 4.0 International license.

to the DRG (Suppl. Fig. 9). Evoked stimuli propagated reliably in both fiber types under control conditions with only occasional failures (basal failure rate in A fibers: 6.3±2.6%, n=8; C fibers: 16.3±2.6%, n=8; Fig. 5B, C), which is consistent with earlier report (18). DRG-applied GABA significantly increased failure rate in C fibers (to 63.8±3.24%, p<0.001) but had no significant effect in A fibers (Fig. 5B, C). Due to technical difficulties of these recordings not all of these were long enough to reliably analyze failure rate but amongst all the recordings made, 89% (34/38) of C fibers and only 24% (11/45) of A-type fibers displayed GABA-induced t-junctional spike failure, while in 100% of both fiber types failure was induced by TTX (Fig. 5D, Suppl. Fig. 9). Taken together, single-unit recordings revealed that DRG application of GABA selectively increases filtering of C-fiber activity.

Soma has more influence over t-junctional filtering in C-type ~~as~~ compared with A-type fibers. DRG neurons are pseudo-unipolar and axonal bifurcation (t-junction) is potentially a major site of spike filtering in DRG due to impedance mismatch (13, 15-17, 31-33). Why is GABA-induced filtering more efficient in the C-fibers, as compared to A-fibers? One possibility is the different length of the stem axon (from the soma to the t-junction) and, thus, the electrotonic influence of the soma on the t-junction and spike propagation: the longer the stem axon, the poorer the coupling (14, 15, 17). To our knowledge, there has been no systematic analysis of stem axon lengths in mammalian DRG neurons, although drawings by Ramon y Cajal depict much shorter stems in small-diameter neurons, as compared to larger ones (34). In addition, larger neurons are often displayed having stems with a glomerular section, extending the length (34, 35). In order to assess stem length in C-type *vs.* A-type fibers we cleared (36) rat whole DRG mounts and immunostained them with the C-fiber marker, peripherin, and A-fiber marker, neurofilament-200 (NF-200). We then performed light-sheet microscopy of entire ganglia (Movie S1) and measured the stem axon lengths of peripherin-positive and NF-200 positive neurons (Movie S2; Fig. 6A-B). Consistently, peripherin labelled neurons with much smaller somatic diameter, as compared to NF-200 positive neurons (26.1±0.4 μm *vs.* 42.4±0.8 μm, p<0.001; Fig. 6A, E; Suppl. Fig. 10). Stem axon diameters of peripherin-labelled neurons were also consistently smaller (1.34±0.03 μm *vs.* 2.1±0.1 μm, p<0.001; Fig. 6D; Suppl. Fig. 10). Peripherin labelled neurons displayed much shorter stems, as compared to NF-200 positive neurons (60.7±4.2 μm *vs.* 232.5±22.9 μm, p<0.001; Fig. 6C; Suppl. Fig. 10). While for all peripherin-positive neurons analyzed in Fig. 6C and Suppl. Fig. 10, the t-junction was reliably identified (Movie S2), it was often impossible to confidently locate the t-junctions of NF-200 positive neurons as these were too far away from the cell body; in these instances stem length was recorded as the longest traceable distance and, hence, it is an underestimation of the real stem length.

We hypothesized that GABAergic control of DRG filtering is less effective in A-fibers compared to C-fibers due to differences in stem axon length. Our previous computational modeling suggested that in a C-fiber with 75 μm stem axon, activation of somatic $GABA_A$ channels can indeed cause a failure of action potential to propagate through the t-junction due to a combination of the impedance drop and sodium channel inactivation (15). But even though data presented in Fig. 6A-C indicate that the stem axon of C-fibers is, on average, at least 3 times shorter than that of A-fibers, myelination could possibly compensate for the longer distance. Using a computational model of an A-fiber neuron, we examined the relationship between somatic conductance and stem axon length. We constructed a minimal model of an A-type neuron (see Suppl. Methods) containing a limited repertoire of voltage-gated channels and a geometry consistent with the parameters obtained from the light-sheet morphometry of the NF-200 positive neurons and compared it to a model with a C-fiber morphology (15).

We first examined the influence of changes in membrane potential at the soma on the t-junction. We calculated the voltage transfer ratio, the fractional potential reaching the t-junction by a potential generated at the soma, as a function of stem axon length (Fig. 6F). In C-fibers, the transfer ratio was greater than 0.75 for a physiological range of stem lengths, while it was less than 0.6 for stem axon lengths measured from A-type neurons. For A-fibers, similar results were obtained by either adjusting the number of internode/node pairs or internode distance. Thus, the modeling predicts that the soma of a C-fiber neuron should have more influence on the t-junction than an A-type neuron soma.

bioRxiv preprint doi: https://doi.org/10.1101/2021.07.14.452325; this version posted July 14, 2021. The copyright holder for this preprint (which was not certified by peer review) is the author/funder, who has granted bioRxiv a license to display the preprint in perpetuity. It is made available under aCC-BY-NC 4.0 International license.

In A-fiber with stem axon of 400 μm, propagating spikes at the nodes of Ranvier were 78-102 mV in amplitude (G_{Na} = 0.5-1 mS/cm^2) and had conduction velocities of 11 m/s for $G_{Na} \geq 1$ S/cm^2. In a C-fiber with a stem axon of 75 μm, propagating spikes were 94-101 mV in amplitude with a maximum conduction velocity of 0.4 m/s (Fig. 6G, left). Through-conduction across a wide range of physiologically-relevant parameter space was not influenced by firing at the soma, consistent with the earlier model (37). To assess the potential effect of $GABA_A$ receptor activation on spike propagation through the DRG, we introduced a chloride conductance (G_{Cl}) in the soma that depolarized the t-junction and reduced local spike amplitude (Fig. 6G, right). The threshold G_{Cl} for blocking spike propagation in the C-fiber model was approximately 10-fold lower than for the A-fiber model. We next systematically examined the relationship between somatic G_{Cl} and G_{Na} (Fig. 6H) and found that spike propagation in this A-fiber model could only be blocked when G_{Na} was less than 0.8 mS/cm^2 and the minimum chloride conductance needed was ~10-fold higher than for the C-fiber model, which was sensitive up to a G_{Na} of 1 mS/cm^2. Taken together, the morphometry of DRG neuron axons and our biophysical model supports the hypothesis that the longer stem axons of A-fibers limit the influence of somatic $GABA_A$ conductances on spike filtering.

Evidence for tonic release of GABA within the DRG. Our paired recordings from SN and DR suggest the existence of tonic filtering at the DRG. There appears to be at least two different types of tonic filtering: in nociceptive fibers it appears to be GABAergic since BIC increases firing rate in the DR (Fig. 1G, H; Suppl. Fig. 1-4) and, when injected to the DRG *in vivo*, induces pain-like behavior (15)). In non-nociceptive fibers it is likely to be mediated by a different mechanism since *i)* poor electrotonic coupling between soma and t-junction (Fig. 6) and *ii)* lack of effect of DRG-applied GABA on basal firing rate in the DR (Suppl. Fig. 1H, I). Here we focused on the GABAergic mechanism; our previous data suggested that some DRG neuron cell bodies are capable of releasing GABA upon stimulation (15). Another recent study reported robust activity-dependent somatic vesicle release from DRG neurons (38). To investigate mechanisms of GABA release by DRG neurons we developed a method for measuring exocytosis of GABA-containing vesicles based on the live uptake of luminal (C-terminal) antibody against vesicular GABA transporter VGAT (Fig. 7A). N-terminus of VGAT, inserted in the neurotransmitter vesicle membrane, faces the cytoplasm while the C terminus resides in the vesicle lumen (39). During exocytosis and subsequent recycling of a vesicle, luminal VGAT epitopes are temporarily exposed to the extracellular milieu. During such an exposure, antibodies that recognize these epitopes can bind to these and become trapped and subsequently internalized by endocytosis (Fig. 7A; (39)). Antibodies against the N-terminus of VGAT should not be entrapped in this way as N-terminus of VGAT remains cytosolic at all times. Depolarization of cultured DRG neurons with extracellular solution containing 100 mM KCl induced robust uptake of C-terminal (luminal) but not N-terminal (cytosolic) VGAT antibody by DRG neurons (Fig. 7B, C; quantified as proportions of neurons stained with the C-terminal VGAT antibody). The depolarization-induced C-terminal VGAT antibody uptake was significantly reduced (but not abolished – in good agreement with (38)) by the removal of extracellular Ca^{2+} (Fig. 7B, C). Interestingly, even in the absence of depolarization, there was a significant number of neurons that took up C-terminal VGAT antibody (Fig. 7B top panel; C), hinting at spontaneous exocytosis of VGAT-containing vesicles. The N-terminal VGAT antibody was not taken up by DRG neurons (Fig. 7B, bottom panel; C), even though this same antibody labeled permeabelized DRG neurons well (15).

Additionally, we used live imaging to optically monitor GABA release from the DRG neurons in culture. We transfected HEK293 cells with α_1, β_2, and γ_2 $GABA_A$ subunits and a halide-sensitive EYFP mutant (H148Q/I152L; EYFP-QL). The fluorescence of EYFP-QL is quenched by iodide and since Cl^- channels (e.g. $GABA_A$) are permeable to this anion, EYFP-QL fluorescence quenching by I^- can be used to monitor Cl^- channel activation (40-43). We co-cultured these 'GABA indicator' HEK293 cells with DRG neurons and measured EYFP-QL fluorescence quenching induced by the addition of 5 mM NaI to the extracellular solution (Fig. 7D). NaI induced robust EYFP-QL fluorescence quenching only when the indicator cells were co-cultured with DRG, not in the monoculture (Fig. 7E). Moreover, this quenching in the DRG/indicator cell co-culture was significantly reduced in the presence of 50 μM BIC (Fig. 7E, F). BIC also significantly

bioRxiv preprint doi: https://doi.org/10.1101/2021.07.14.452325; this version posted July 14, 2021. The copyright holder for this preprint (which was not certified by peer review) is the author/funder, who has granted bioRxiv a license to display the preprint in perpetuity. It is made available under aCC-BY-NC 4.0 International license.

slowed down the kinetics of the EYFP-QL fluorescence intensity decay (Fig. 7G). These data further support existence of GABA tone in DRG.

Discussion.

There is substantial evidence indicating that spinal ganglia regulate the flow of sensory information through to the CNS and that this processing can be modulated by GABAergic signalling. Thus, it was shown that DRG neurons can produce and release inhibitory neurotransmitter GABA (15, 23), GABA delivered specifically into the DRG has prominent analgesic action (15, 22) and that electrical stimulation of DRGs provides strong analgesia even to the most intractable types of chronic pain in humans (44-46). Experimental measurements (13, 14, 18, 19, 47-49) and simulations (14-17, 50) suggested axonal t-junctions as biophysically amenable sites for peripheral filtering/gating and modulation by intrinsic GABA signalling.

Our main findings here are twofold. First, we demonstrate that the DRG exerts a dynamic control over the throughput conduction via GABA receptor activation. Second, we show that this control is much more efficient in the C-fibers, as compared to A-fibers. Thus, we demonstrate that an intrinsic GABAergic inhibitory system can be engaged to scale the filtering of spikes passing through the DRG up or down, modulating nociceptive input to the CNS. Indeed, focal application of GABA, or optogenetic stimulation of GABA release from the DRG-transplanted MGE cells, specifically reduced stimulus-induced firing frequencies in the DR but not the SN aspects of the nerve in various experimental settings.

The t-junction, where the stem axon bifurcates into SN and DR axons, are expected to have a lowered safety factor for AP propagation due to the impedance mismatch (13-15, 32, 48, 51). Our earlier biophysical model of a C-fiber predicted that opening of somatic/peri-somatic $GABA_A$ channels promotes failure of action potential propagation through the t-junction due to a combination of input impedance drop, GABA conductance shunting, and voltage-gated sodium channel inactivation (15). Here we provide strong experimental support to these predictions. We show that GABA receptor activation within the DRG reduces the evoked firing rate recorded at a point immediately after the t-junction, and has no effect on spikes entering the DRG. The most straightforward interpretation of these observations is that evoked spikes in peripheral axons fail to propagate through the DRG into DR axons when GABA system is activated in the DRG.

Another striking finding is that DRG filtering is much more robust in C-, as compared to the A-fibers. As a consequence, optogenetic GABA release (Suppl. Fig. 7) or DRG injection of GABA (Suppl. Fig. 8) specifically inhibited firing produced by noxious but not innocuous stimuli. Interestingly, a recent study used single unit recordings from the DR to demonstrate that electric field stimulation of the DRG in rats increases t-junctional filtering mostly in C-fibers, with little effect in A-type fibers (19). These findings are in good agreement with our results and likely to represent a related phenomenon. We propose that the induced filtering is more efficient in the C-fibers because these have a shorter stem axon. Electrotonic coupling of the soma to the t-junction depends on the stem axon length (15, 17). Drawings by Ramon y Cajal indeed suggested much shorter stems in small-diameter DRG neurons, as compared to the larger ones (34). Our light-sheet imaging of cleared DRG with labelled C- and A-type fibers established that stem axon is indeed over 3 times shorter in C fibers (Fig. 6). Our new biophysical model of an A-fiber suggests that when a stem axon is longer than 200-300 μm, opening of somatic $GABA_A$ channels has minimal effect on the action potentials propagating through their t-junctions. Thus, this investigation may have revealed a simple but elegant principle of differential filtering of spikes that depends on the modality-specific fiber morphology. It has to be acknowledged that other mechanisms, e.g. differential ion channel densities (including but not limited to $GABA_A$) at the t-junctions or stem axon of different fiber types could also contribute to the differential filtering.

Two consistent, but yet to be fully understood, observations reported here require further consideration. First, there was considerable basal activity under control (no peripheral stimulation) conditions. This was unexpected and may arise from the preparation-specific injury. However, our previous observation that DRG-injected GABA antagonists in freely behaving animals induced pain-like paw flinching in the absence of noxious input (15) may suggest that there is indeed some tonic activity in the peripheral nerve which is failing to reach spinal cord.

bioRxiv preprint doi: https://doi.org/10.1101/2021.07.14.452325; this version posted July 14, 2021. The copyright holder for this preprint (which was not certified by peer review) is the author/funder, who has granted bioRxiv a license to display the preprint in perpetuity. It is made available under aCC-BY-NC 4.0 International license.

Second, basal firing rates in the DR were almost invariantly about 50% lower, as compared to these in SN, even under conditions where efferent fibers were either cut (Suppl. Fig. 1) or physically destroyed (Suppl. Fig. 2). Single-unit recordings (Fig. 5) revealed that evoked spikes in C and A fibers do fail occasionally under basal conditions (at a rate of ~16% in C and ~6% in A fibers), which was consistent with a recent report (18). Thus, basal filtering does exist but when measuring evoked single-unit spikes it is much lower than ~50% mismatch seen in our multi-unit SN/DR recordings. While $GABA_A$ antagonist BIC significantly reduced this mismatch indicating that at least part of it is due to tonic GABAergic inhibition, we cannot exclude that other factors may contribute to the mismatch, including e.g. some back-propagation in the SN. It is important to note however that regardless of the nature of this mismatch in basal firing, the sensory stimulation of the paw (noxious or innocuous) is seen in our SN/DR recordings as a consistent increase in the firing rates in both compartments (SN and DR). Moreover, we were able to identify individual capsaicin-induced units using our spike matching algorithm (Fig. 2, Suppl. Fig. 5). Thus, the activity induced by noxious stimulation is reliably detectable on the background of the basal activity. Importantly, it is this induced noxious activity, which is specifically filtered at the DRG by the GABAergic system.

Another important question - is the intrinsic GABAergic system in the DRG sufficient to impose filtering *in vivo*? Strong expression of functional $GABA_A$ receptors in DRG is well recognized (reviewed in (52)) but the ability of DRG to produce and release GABA is less well documented (although see (15, 23). Transcript levels of enzymes (GAD65, GAD67) and transporters (VGAT) needed to synthesize and package GABA into vesicles are low according to transcriptomic studies (53, 54). Yet functional proteins are detectable (15, 23, 55), as is tonic and induced GABA release (Fig. 7 and (15)). It has to be pointed that a non-vesicular mechanism for GABA release that does not require VGAT also exists (i.e. via LRRC8 channels (56)). Another important evidence for endogenous GABA tone is the *in vivo* studies that demonstrated that GABA reuptake inhibitor, NO711, produced analgesic effect when delivered to the DRG *in vivo* (15, 22). DRG-applied $GABA_A$ antagonists, on the other hand, exacerbated peripherally-induced pain and even produced a pain-like behaviour (15). Hence, there must be sufficient amount of endogenous GABA in the DRG to control the 'filter'.

A major causative factor of neuropathic pain is a loss of dorsal horn GABAergic inhibitory system (57). GABAergic progenitor cells implanted into adult spinal cord survive and integrate into the spinal inhibitory circuit (27, 58, 59), reducing neuropathic pain severity (26, 60). We found the MGE cells transplanted into the DRG of adult mice also survive there and can release GABA (Fig. 3). Optogenetic stimulation of MGE-transplanted DRG significantly alleviated chronic inflammatory hyperalgesia (Fig. 3). Importantly, even without optogenetic stimulation, MGE cell transplantation accelerated the recovery from both inflammatory and neuropathic types of hyperalgesia (Suppl. Fig. 6). This, together with observed higher efficiency of GABAergic filtering at the C, as compared to A fibers could have a therapeutic significance as it suggests that GABAergic system in DRG could be targeted for pain relief without significantly compromising other haptic sensations. In the spinal cord MGE cells maturate into interneurons and integrate into the existing spinal inhibitory system (26, 27). For the case of the DRG transplant, the direct analogy is unlikely as there are no 'classical' interneurons in DRG. The most straightforward explanation for the anti-nociceptive effect of MGE cells in DRG is a 'GABA pump' mechanism, whereby MGE cells simply leak GABA into the extracellular space. Recent years saw increasing success in using stem cells as a chronic pain therapy (61, 62) and GABAergic progenitor cells can be generated from human stem cells (63) and integrated into the pain pathways (64). Thus, targeting GABAergic system with the DRG-directed stem cell therapy or GABA-mimetics tailored to reduce their CNS permeability could open up avenues for analgesic strategies with reduced CNS side effects.

bioRxiv preprint doi: https://doi.org/10.1101/2021.07.14.452325; this version posted July 14, 2021. The copyright holder for this preprint (which was not certified by peer review) is the author/funder, who has granted bioRxiv a license to display the preprint in perpetuity. It is made available under aCC-BY-NC 4.0 International license.

Materials and Methods

All animal experiments were performed with the approval of the Animal Care and Ethics Committee of Hebei Medical University under the International Association for the Study of Pain guidelines.

***In vivo* recording of peripheral nerve activity.** All surgical procedures were performed under deep anesthesia with an i.p. injection of pentobarbital sodium (60 - 80 mg/kg) in accordance with the Animal Care and Ethical Committee of Hebei Medical University under the International Association for the Study of Pain guidelines. In one set of experiments (Suppl. Fig. 4) pentobarbital was replaced by isoflurane (4% for induction, 2% for maintenance). Laminectomy was performed to expose right L5 DRG of adult rat (Sprague-Dawley, 180-200 g) or L4 DRG of adult C57BL/6J mice. Male animals were used in experiments, except where stated otherwise. Dorsal root (DR), spinal nerve (SN) and DRG were exposed by removal of both spinous and transverse processes of the vertebra bone; the DR and SN were then suspended on the hooked stainless-still recording electrodes connected to BL-420F biological data acquisition and analysis system (Chengdu Techman Software Co., Ltd. China). The wound was filled with paraffin in order to stabilize preparation. The right hindpaw was used for the injection of capsaicin (10 μM; 50 μl for rat; 20 μl for mouse) or Bradykinin (100 μM, 50 μl for rat; 20 μl for mouse), or the stimulation with hot water (~60°C), ice, air puffs (using aurilave), von Frey filaments (4 g for rat; 0.4 g for mouse) or needle prick (glass electrode). GABA (200 μM; 3 μl for rat; 2 μl for mouse) or Bicuculline (200 μM; 3 μl for rat; 2 μl for mouse) was accurately delivered to DRG by micropipettor.

For the single unit recording in rats, dorsal root and spinal nerve were exposed and covered with paroline. A single fiber was teased away from dorsal root by microscopic tweezer and placed on nerve fiber electrode for electrophysiological recording. The stimulus current delivered to the spinal nerve was gradually raised (10 Hz, 2 - 5 mA). Conduction velocity of fiber was determined by dividing conduction distance by response latency to electrical stimulus. GABA (200 μM, 3 μl) or Tetrodotoxin (TTX, 1 μM, 3 μl) was accurately delivered to DRG by micropipettor.

Spike sorting. Electrophysiological recordings of both the spinal nerve and dorsal root were imported into Python and high pass filtered at 60 Hz using a digital Butterworth filter from the Scipy module (65). Extracellular spike times and waveforms were extracted using an absolute median deviation of between 5 and 6 from the median of the signal. Extracted spike waveforms were sorted using the WaveClus program (66) in Matlab to define individual neuronal units underlying the extracellular signal. Matching of spikes in the dorsal root to an origin spike in the spinal nerve was achieved by finding the minimum latency (within a tolerance window of the slowest theoretical fibre conduction velocity of 0.1 m/s) between spikes in the spinal nerve and dorsal root. Propagation failure was defined when a spinal nerve spike did not have a matching dorsal root spike within the tolerance window.

MGE cells transplantation. The female VGAT-ChR2-EYFP mice (Jackson Laboratory) with embryos between E12.5 and E13.5 were anesthetized with an intraperitoneal injection of pentobarbital sodium (60-80 mg/kg). All the embryos were removed via abdominal incision and placed into a 10 cm Petri dish containing ice-cold HBSS. The mice were humanely sacrificed. The gestational sac of each embryo was removed using forceps under the stereo microscope (SZX7, Olympus). The embryonic brain was extracted and cut along the sagittal plane to separate two hemispheres. Medial ganglionic eminence (MGE) on each hemisphere was then removed with a scalpel. MGE tissue was put in a 1.5 ml collection tube containing 500 □l DMEM/10% FBS (Sigma) and triturated into a single cell suspension as described (67). The final cell density in the suspension of embryonic stem cells was measured with hemocytometer. Adult **(**5-6 weeks) male C57BL/6J mice were anesthetized with an intraperitoneal injection of pentobarbital sodium (60 - 80 mg/kg). L4 DRG was exposed by removal of both spinous and transverse processes of the vertebra bone. The microinjector (Hamilton Co.) loaded with a suspension of MGE cells (3 μl; ~1x10^{7}/ml) was inserted into the ganglion to a depth of 200 μm from the exposed surface. The cell suspension was injected slowly, and the needle was removed 3 minutes after the injection.

bioRxiv preprint doi: https://doi.org/10.1101/2021.07.14.452325; this version posted July 14, 2021. The copyright holder for this preprint (which was not certified by peer review) is the author/funder, who has granted bioRxiv a license to display the preprint in perpetuity. It is made available under aCC-BY-NC 4.0 International license.

The muscles overlying the spinal cord were loosely sutured together, and the wound was closed. Animals developing signs of distress were humanely sacrificed. In order to verify that the DRGs were transplanted with MGE cells successfully, the L4 DRGs were excised, submerged in Tissue-Tek O.C.T. (Sakura, Alphen aan den Rijn, The Netherlands), frozen, and sectioned (10 µm) using a freezing microtome (CM1950, Leica Microsystems). Slices were then analyzed for the EYFP fluorescence using confocal microscopy (TCS SP5 II, Leica Microsystems).

Chronic pain models and Behavioral tests. Chronic constriction injury (CCI) and mechanical and thermal sensitivity tests were performed as described previously (15), further details are provided in Supplementary Methods.

***In vivo* optogenetic stimulation.** Adult male C57BL/6J mice were L4 DRG transplanted with MGE cells from VGAT-ChR2-EYFP mice 3-4 weeks before experiments. Recordings of DR and SN activity was performed as described above in combination with laser stimulation (473 nm, 3 mW, 30 Hz for 10 seconds with 20-second interval) of DRG using an MLL-FN-473-50 unit (Changchun New Industries Optoelectronics Technology Co., Ltd.) controlled by a pulsing set (S48 Stimulator, Grass Technologies, An Astro-Med, Inc. Product Group). In the behavioral tests on freely moving animals, a stainless steel cannula guide (RWD Life Science Co. Ltd., China; diameter 0.64 mm) was implanted the L4 DRG, the cannula was firmly fixed in place with dental cement, and the optical fiber (RWD Life Science Co. Ltd., China; diameter 0.2 mm, length 1 m) was inserted through the guide; a more detailed description is provided in (15).

Patch clamp recording from DRG neurons. Patch clamp recording from DRG neurons. DRG dissection and recording were performed as described previously (68), further details are provided in Supplementary Methods.

VGAT antibody uptake. DRG neurons were dissociated and cultured as described previously (68). DRG neurons were incubated for 15 min in either normal or 'high K^{+}' extracellular (EC) solution supplemented with either C-terminal (luminal) N-terminal (cytosolic) VGAT antibodies. Normal EC solution contains (in mM): 144 NaCl, 5.8 KCl, 1.3 $CaCl_2$, 5.6 D-glucose, 0.7 NaH_2PO4, 0.9 $MgCl_2$ and 10 HEPES (all from Sigma). In high K^+ EC solution NaCl concentration was lowered to 49.8 mM and KCl concentration was raised to 100 mM. Ca^{2+}-free EC solution was also used; in this solution $CaCl_2$ was omitted. After incubation cell cultures were washed 3 times with PBS and fixed using 4% paraformaldehyde, followed by permeabilization with 0.05% tween 20 and 0.25% triton-X 100 (with donkey serum) for 1 hr. Cells were then labelled with secondary antibody, washed three times with PBS, mounted on coverslips and imaged using Zeiss LSM880 confocal microscope. The following antibodies were used: VGAT C-terminal antibody (rabbit polyclonal #AB-N44, Advance Targeting System; 1:200); VGAT N-terminal antibody (rabbit polyclonal 131002, Invitrogen, Eugene, Oregon, USA; 1:1000); secondary antibody: alexafluor donkey anti-rabbit 488 (Invitrogen, Eugene, Oregon, USA; 1:1000).

Iodide imaging. HEK293 cells were co-transfected with cDNA encoding human α1, β2 and γ2 subunits of $GABA_A$ receptors (gift of David Weiss, Department of Physiology, University of Texas Health Science Center, San Antonio, Texas, USA) together with the halide-sensitive EYFP mutant (H148Q/I152L; EYFP-QL) using FuGENE® HD transfection reagent. Transfected cells were co-cultured for 24 hrs with DRG neurons isolated as described above (see also (15)). Extracellular solution consisted of (mM): NaCl (160); KCl (2.5); $MgCl_2$ (1); $CaCl_2$ (2); HEPES (10) and Glucose (10); pH adjusted to 7.4 with NaOH (All from Sigma). I^- containing solution was produced by equimolar substitution of 5 mM NaCl with NaI. I^- imaging was performed using Nikon TE-2000 E Swept Field Confocal microscope using 488nm argon laser as excitation light source. Images were recorded and analyzed using Nikon Elements software.

Dorsal root ganglia clearing, staining and morphometry. DRGs tissue clearing was performed using the iDISCO+ protocol (36). Cleared DRG samples were imaged using Ultramicroscope II (LaVision BioTech) Images were analyzed using the simple neurite tracer in FIJI. Using this semi-automatic method of tracing (Movie S2), stem axons were measured from origin at peripherin and NF-200-positive somata through the image stack until clear bifurcation or in the case of NF-200-positive cells, loss of a clear signal. Further details are provided in Supplementary Methods.

bioRxiv preprint doi: https://doi.org/10.1101/2021.07.14.452325; this version posted July 14, 2021. The copyright holder for this preprint (which was not certified by peer review) is the author/funder, who has granted bioRxiv a license to display the preprint in perpetuity. It is made available under aCC-BY-NC 4.0 International license.

Computer modelling. All simulations were performed using NEURON (69) on an Intel-based Macintosh computer (http://neuron.yale.edu) and analyzed using Python scripts; further details are provided in Supplementary Methods.

Statistics. All data are given as mean ± SEM. Paired or unpaired t-test was used to compare the mean of two groups when the data were normally distributed. Multiple groups were compared using ANOVA (one-, two- or three-factor) or repeated-measures ANOVA, depending on experimental setup; Bonferroni post-hoc test was used for comparison between groups; for data failing normality test Kruskal-Wallis ANOVA with Mann-Whitney post-hoc test was used. Statistical analyses were performed using IBM SPSS Statistics 21, GraphPad Prism or Origin. Statistical parameters are given in the figure legends.

Acknowledgments

We thank Prof Jim Deuchars and Dr Ronaldo Ichiyama (University of Leeds) for advice on experiments. We also thank Dr Junling Xing (Fourth Military Medical University) for help with setting up single unit recordings. This work was supported by the National Natural Science Foundation of China grants (84870872 & 313400048), Key Basic Research Project of Applied Basic Research Program of Hebei Province (16967712D) and Science Fund for Creative Research Groups of Natural Science Foundation of Hebei Province (H2020206474) to X.D.; National Natural Science Foundation of China (91732108, 81871075) grants to H.Z.; Innovation fund for graduate students of Hebei Province (CXZZBS2018077) to H.H.; the Wellcome Trust Investigator Award 212302/Z/18/Z to N.G.

References

1. R. Melzack, P. D. Wall, Pain mechanisms: a new theory. *Science* **150**, 971-979 (1965).
2. J. Braz, C. Solorzano, X. Wang, A. I. Basbaum, Transmitting pain and itch messages: a contemporary view of the spinal cord circuits that generate gate control. *Neuron* **82**, 522-536 (2014).
3. L. M. Mendell, Constructing and deconstructing the gate theory of pain. *Pain* **155**, 210-216 (2014).
4. B. Duan *et al.*, Identification of spinal circuits transmitting and gating mechanical pain. *Cell* **159**, 1417-1432 (2014).
5. H. B. Barlow, "Possible principles underlying the transformations of sensory messages" in Sensory Communication, W. Rosenblith, Ed. (M.I.T. Press, 1961), pp. 782-790.
6. R. F. Schmidt, "The gate control theory of pain. An unlikely hypothesis" in Pain, R. Janzen, Keidel, W.D., Herz, A., Steichele, C. , Ed. (London: Churchill Livingstone, 1972), pp. 124–127.
7. P. W. Nathan, The gate-control theory of pain. A critical review. *Brain* **99**, 123-158 (1976).
8. R. A. Meyer, S. N. Raja, J. N. Campbell, Coupling of action potential activity between unmyelinated fibers in the peripheral nerve of monkey. *Science* **227**, 184-187 (1985).
9. R. A. Meyer, S. N. Raja, J. N. Campbell, S. E. Mackinnon, A. L. Dellon, Neural activity originating from a neuroma in the baboon. *Brain Res* **325**, 255-260 (1985).
10. R. Amir, M. Devor, Chemically mediated cross-excitation in rat dorsal root ganglia. *J Neurosci* **16**, 4733-4741 (1996).
11. R. Amir, M. Devor, Functional cross-excitation between afferent A- and C-neurons in dorsal root ganglia. *Neuroscience* **95**, 189-195 (2000).
12. Y. S. Kim *et al.*, Coupled Activation of Primary Sensory Neurons Contributes to Chronic Pain. *Neuron* **91**, 1085-1096 (2016).
13. G. Gemes *et al.*, Failure of action potential propagation in sensory neurons: mechanisms and loss of afferent filtering in C-type units after painful nerve injury. *J Physiol* **591**, 1111-1131 (2013).
14. X. Du *et al.*, Control of somatic membrane potential in nociceptive neurons and its implications for peripheral nociceptive transmission. *Pain* **155**, 2306-2322 (2014).

bioRxiv preprint doi: https://doi.org/10.1101/2021.07.14.452325; this version posted July 14, 2021. The copyright holder for this preprint (which was not certified by peer review) is the author/funder, who has granted bioRxiv a license to display the preprint in perpetuity. It is made available under aCC-BY-NC 4.0 International license.

15. X. Du *et al.*, Local GABAergic signaling within sensory ganglia controls peripheral nociceptive transmission. *J Clin Invest* **127**, 1741-1756 (2017).
16. A. R. Kent, X. Min, Q. H. Hogan, J. M. Kramer, Mechanisms of Dorsal Root Ganglion Stimulation in Pain Suppression: A Computational Modeling Analysis. *Neuromodulation* **21**, 234-246 (2018).
17. D. Sundt, N. Gamper, D. B. Jaffe, Spike propagation through the dorsal root ganglia in an unmyelinated sensory neuron: a modeling study. *J Neurophysiol* **114**, 3140-3153 (2015).
18. D. Al-Basha, S. A. Prescott, Intermittent Failure of Spike Propagation in Primary Afferent Neurons during Tactile Stimulation. *J Neurosci* **39**, 9927-9939 (2019).
19. D. Chao, Z. Zhang, C. M. Mecca, Q. H. Hogan, B. Pan, Analgesic dorsal root ganglionic field stimulation blocks conduction of afferent impulse trains selectively in nociceptive sensory afferents. *Pain* **161**, 2872-2886 (2020).
20. P. D. Wall, Cord cells responding to touch, damage, and temperature of skin. *J Neurophysiol* **23**, 197-210 (1960).
21. W. Janig, R. F. Schmidt, M. Zimmermann, Single unit responses and the total afferent outflow from the cat's foot pad upon mechanical stimulation. *Exp Brain Res* **6**, 100-115 (1968).
22. A. L. Obradovic *et al.*, Silencing the alpha2 subunit of gamma-aminobutyric acid type A receptors in rat dorsal root ganglia reveals its major role in antinociception posttraumatic nerve injury. *Anesthesiology* **123**, 654-667 (2015).
23. C. Hanack *et al.*, GABA blocks pathological but not acute TRPV1 pain signals. *Cell* **160**, 759-770 (2015).
24. T. X. Hoang, J. H. Nieto, N. J. Tillakaratne, L. A. Havton, Autonomic and motor neuron death is progressive and parallel in a lumbosacral ventral root avulsion model of cauda equina injury. *J Comp Neurol* **467**, 477-486 (2003).
25. M. Koltzenburg, C. L. Stucky, G. R. Lewin, Receptive properties of mouse sensory neurons innervating hairy skin. *J Neurophysiol* **78**, 1841-1850 (1997).
26. J. M. Braz *et al.*, Forebrain GABAergic neuron precursors integrate into adult spinal cord and reduce injury-induced neuropathic pain. *Neuron* **74**, 663-675 (2012).
27. A. Etlin *et al.*, Functional Synaptic Integration of Forebrain GABAergic Precursors into the Adult Spinal Cord. *J Neurosci* **36**, 11634-11645 (2016).
28. M. Rigaud *et al.*, Species and strain differences in rodent sciatic nerve anatomy: implications for studies of neuropathic pain. *Pain* **136**, 188-201 (2008).
29. L. Li *et al.*, The functional organization of cutaneous low-threshold mechanosensory neurons. *Cell* **147**, 1615-1627 (2011).
30. V. E. Abraira, D. D. Ginty, The sensory neurons of touch. *Neuron* **79**, 618-639 (2013).
31. S. S. Goldstein, W. Rall, Changes of action potential shape and velocity for changing core conductor geometry. *Biophys J* **14**, 731-757 (1974).
32. C. Luscher, J. Streit, R. Quadroni, H. R. Luscher, Action potential propagation through embryonic dorsal root ganglion cells in culture. I. Influence of the cell morphology on propagation properties. *J Neurophysiol* **72**, 622-633 (1994).
33. D. Debanne, E. Campanac, A. Bialowas, E. Carlier, G. Alcaraz, Axon physiology. *Physiol Rev* **91**, 555-602 (2011).
34. S. Ramón y Cajal, *Histologie du système nerveux de l'homme & des vertébrés* (Paris : Maloine, 1909), vol. 1.
35. S. Matsuda *et al.*, Phylogenetic investigation of Dogiel's pericellular nests and Cajal's initial glomeruli in the dorsal root ganglion. *J Comp Neurol* **491**, 234-245 (2005).
36. N. Renier *et al.*, Mapping of Brain Activity by Automated Volume Analysis of Immediate Early Genes. *Cell* **165**, 1789-1802 (2016).
37. R. Amir, M. Devor, Electrical excitability of the soma of sensory neurons is required for spike invasion of the soma, but not for through-conduction. *Biophys J* **84**, 2181-2191 (2003).
38. Z. Chai *et al.*, CaV2.2 Gates Calcium-Independent but Voltage-Dependent Secretion in Mammalian Sensory Neurons. *Neuron* **96**, 1317-1326 e1314 (2017).
39. H. Martens *et al.*, Unique luminal localization of VGAT-C terminus allows for selective labeling of active cortical GABAergic synapses. *J Neurosci* **28**, 13125-13131 (2008).
40. L. J. Galietta, P. M. Haggie, A. S. Verkman, Green fluorescent protein-based halide indicators with improved chloride and iodide affinities. *FEBS Lett* **499**, 220-224 (2001).

bioRxiv preprint doi: https://doi.org/10.1101/2021.07.14.452325; this version posted July 14, 2021. The copyright holder for this preprint (which was not certified by peer review) is the author/funder, who has granted bioRxiv a license to display the preprint in perpetuity. It is made available under aCC-BY-NC 4.0 International license.

41. T. Johansson, T. Norris, H. Peilot-Sjogren, Yellow fluorescent protein-based assay to measure GABA(A) channel activation and allosteric modulation in CHO-K1 cells. *PLoS One* **8**, e59429 (2013).
42. W. Namkung, Z. Yao, W. E. Finkbeiner, A. S. Verkman, Small-molecule activators of TMEM16A, a calcium-activated chloride channel, stimulate epithelial chloride secretion and intestinal contraction. *FASEB J* **25**, 4048-4062 (2011).
43. S. Shah *et al.*, Local Ca^{2+} signals couple activation of TRPV1 and ANO1 sensory ion channels. *Sci Signal* **13**, eaaw7963 (2020).
44. T. R. Deer, E. Grigsby, R. L. Weiner, B. Wilcosky, J. M. Kramer, A prospective study of dorsal root ganglion stimulation for the relief of chronic pain. *Neuromodulation* **16**, 67-71 (2013).
45. L. Liem *et al.*, A Multicenter, Prospective Trial to Assess the Safety and Performance of the Spinal Modulation Dorsal Root Ganglion Neurostimulator System in the Treatment of Chronic Pain. *Neuromodulation* **16**, 471-482 (2013).
46. C. W. Hunter *et al.*, DRG FOCUS: A Multicenter Study Evaluating Dorsal Root Ganglion Stimulation and Predictors for Trial Success. *Neuromodulation* **22**, 61-79 (2019).
47. F. T. Dun, The delay and blockage of sensory impulses in the dorsal root ganglion. *J Physiol* **127**, 252-264 (1955).
48. S. D. Stoney, Jr., Unequal branch point filtering action in different types of dorsal root ganglion neurons of frogs. *Neurosci Lett* **59**, 15-20 (1985).
49. G. Tagini, E. Camino, T-shaped cells of dorsal ganglia can influence the pattern of afferent discharge. *Pflugers Arch* **344**, 339-347 (1973).
50. C. Luscher, J. Streit, P. Lipp, H. R. Luscher, Action potential propagation through embryonic dorsal root ganglion cells in culture. II. Decrease of conduction reliability during repetitive stimulation. *J Neurophysiol* **72**, 634-643 (1994).
51. D. Debanne, Information processing in the axon. *Nat Rev Neurosci* **5**, 304-316 (2004).
52. B. U. Wilke, K. K. Kummer, M. G. Leitner, M. Kress, Chloride - The Underrated Ion in Nociceptors. *Front Neurosci* **14**, 287 (2020).
53. S. E. Jager *et al.*, Changes in the transcriptional fingerprint of satellite glial cells following peripheral nerve injury. *Glia* **68**, 1375-1395 (2020).
54. D. Usoskin *et al.*, Unbiased classification of sensory neuron types by large-scale single-cell RNA sequencing. *Nat Neurosci* **18**, 145-153 (2015).
55. H. R. Tzeng *et al.*, alpha6GABAA Receptor Positive Modulators Alleviate Migraine-like Grimaces in Mice via Compensating GABAergic Deficits in Trigeminal Ganglia. *Neurotherapeutics* **18**, 569-585 (2021).
56. D. Lutter, F. Ullrich, J. C. Lueck, S. Kempa, T. J. Jentsch, Selective transport of neurotransmitters and modulators by distinct volume-regulated LRRC8 anion channels. *J Cell Sci* **130**, 1122-1133 (2017).
57. K. A. Moore *et al.*, Partial peripheral nerve injury promotes a selective loss of GABAergic inhibition in the superficial dorsal horn of the spinal cord. *J Neurosci* **22**, 6724-6731 (2002).
58. I. J. Llewellyn-Smith, A. I. Basbaum, J. M. Braz, Long-term, dynamic synaptic reorganization after GABAergic precursor cell transplantation into adult mouse spinal cord. *J Comp Neurol* **526**, 480-495 (2018).
59. J. M. Braz, A. Etlin, D. Juarez-Salinas, I. J. Llewellyn-Smith, A. I. Basbaum, Rebuilding CNS inhibitory circuits to control chronic neuropathic pain and itch. *Progress in brain research* **231**, 87-105 (2017).
60. J. M. Braz, X. Wang, Z. Guan, J. L. Rubenstein, A. I. Basbaum, Transplant-mediated enhancement of spinal cord GABAergic inhibition reverses paclitaxel-induced mechanical and heat hypersensitivity. *Pain* **156**, 1084-1091 (2015).
61. I. Hwang *et al.*, Intrathecal Transplantation of Embryonic Stem Cell-Derived Spinal GABAergic Neural Precursor Cells Attenuates Neuropathic Pain in a Spinal Cord Injury Rat Model. *Cell Transplant* **25**, 593-607 (2016).
62. H. Yu *et al.*, Analgesia for neuropathic pain by dorsal root ganglion transplantation of genetically engineered mesenchymal stem cells: initial results. *Mol Pain* **11**, 5 (2015).
63. Y. Liu *et al.*, Medial ganglionic eminence-like cells derived from human embryonic stem cells correct learning and memory deficits. *Nat Biotechnol* **31**, 440-447 (2013).

bioRxiv preprint doi: https://doi.org/10.1101/2021.07.14.452325; this version posted July 14, 2021. The copyright holder for this preprint (which was not certified by peer review) is the author/funder, who has granted bioRxiv a license to display the preprint in perpetuity. It is made available under aCC-BY-NC 4.0 International license.

64. J. Manion *et al.*, Human induced pluripotent stem cell-derived GABAergic interneuron transplants attenuate neuropathic pain. *Pain* **161**, 379-387 (2020).
65. P. Virtanen *et al.*, SciPy 1.0: fundamental algorithms for scientific computing in Python. *Nat Methods* **17**, 261-272 (2020).
66. F. J. Chaure, H. G. Rey, R. Quian Quiroga, A novel and fully automatic spike-sorting implementation with variable number of features. *J Neurophysiol* **120**, 1859-1871 (2018).
67. D. Vogt *et al.*, Viral-mediated Labeling and Transplantation of Medial Ganglionic Eminence (MGE) Cells for In Vivo Studies. *J Vis Exp* 10.3791/52740 (2015).
68. B. Liu *et al.*, The acute nociceptive signals induced by bradykinin in rat sensory neurons are mediated by inhibition of M-type K^+ channels and activation of Ca^{2+}-activated Cl^- channels. *J Clin Invest* **120**, 1240-1252 (2010).
69. M. L. Hines, N. T. Carnevale, NEURON: a tool for neuroscientists. *Neuroscientist* **7**, 123-135 (2001).

bioRxiv preprint doi: https://doi.org/10.1101/2021.07.14.452325; this version posted July 14, 2021. The copyright holder for this preprint (which was not certified by peer review) is the author/funder, who has granted bioRxiv a license to display the preprint in perpetuity. It is made available under aCC-BY-NC 4.0 International license.

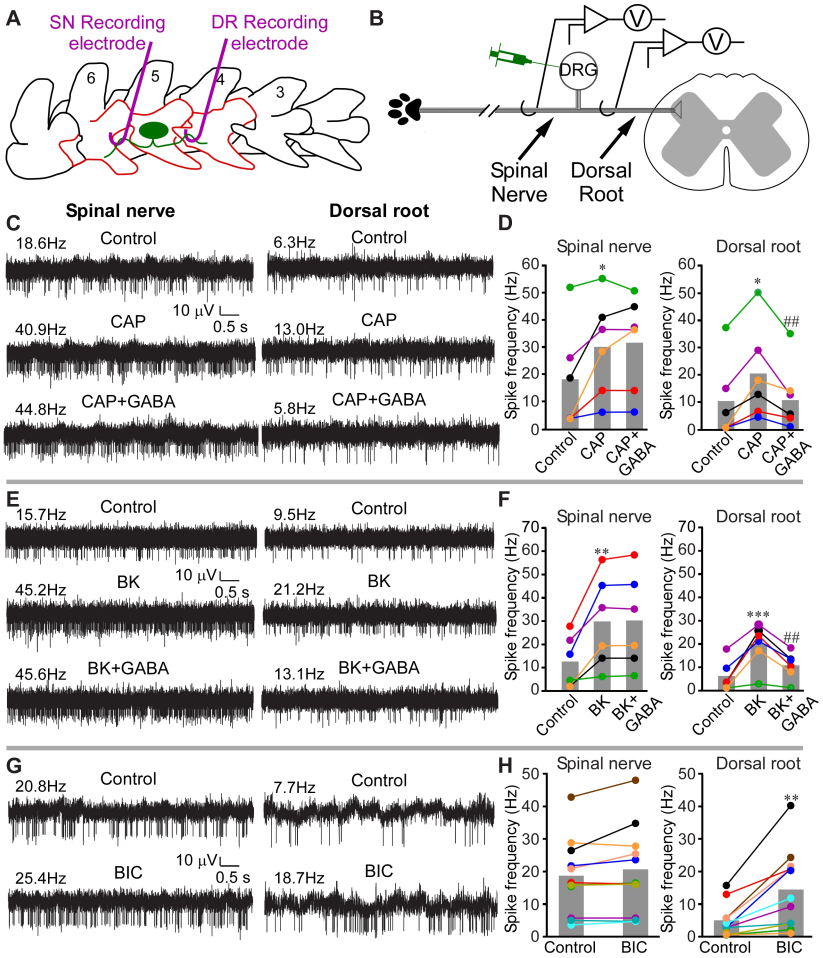

Figure 1

bioRxiv preprint doi: https://doi.org/10.1101/2021.07.14.452325; this version posted July 14, 2021. The copyright holder for this preprint (which was not certified by peer review) is the author/funder, who has granted bioRxiv a license to display the preprint in perpetuity. It is made available under aCC-BY-NC 4.0 International license.

Figure 1. GABAergic filtering of nociceptive signals at the DRG. (**A**) Schematic of surgical exposure of the L5 spinal nerve (SN, left), L5 DRG and the dorsal root (DR, middle) in an anesthetized rat. Parts of the vertebra that are surgically removed are shown in orange. SN and DR are then individually suspended on fine hook electrodes; DRG is exposed to direct drug application. (**B**), schematic of the electrode placement. (**C**) Hindpaw injection of Capsaicin (CAP, 10 μM, 50 μl) increased firing frequency in both SN and DR branches of the nerve (middle traces, as compared to basal activity shown in the upper traces). Application of GABA (200 μM, 3 μl) to DRG reduced CAP-induced firing frequency in DR but not SN (bottom traces). (**D**) Summary of panel C. Two-factor repeated measures ANOVA, with factors of nerve site (SN, DR) and drug treatment (Control, CAP, CAP+GABA) revealed main effects associated with nerve site [$F(1,5)=15.1$; $p<0.05$] and drug application [$F(2,4)=12.8$; $p<0.05$], and there was significant interaction between these factors [$F(2,4)=7.9$; $p<0.05$]. Bonferroni post-hoc test: *significant difference from control ($p<0.05$); ##significant difference from CAP ($p<0.01$). (**E**), similar to C, but Bradykinin (BK, 100 μM, 50 μl) was hindpaw injected, instead of CAP. (**F**) Summary of panel E. Two-factor repeated measures ANOVA: main effect associated with drug application [$F(2,4)=12.0$; $p<0.05$]; significant interaction between nerve site and drug application [$F(2,4)=11.5$; $p<0.05$]. Bonferroni post-hoc test: **,***significant difference from control ($p<0.01$, $p<0.001$); ##significant difference from BK ($p<0.01$). (**G**) $GABA_A$ antagonist bicuculline (BIC, 200 μM, 3 μl) was applied to DRG instead of GABA; hindpaw was not stimulated. (**H**) Summary of panel G. Two-factor repeated measures ANOVA: main effects associated with nerve site [$F(1,10)=7.7$; $p<0.05$), drug application [$F(1,10)=12.0$; $p<0.01$), significant interaction between nerve site and drug application [$F(1,10)=18.7$; $p<0.01$]. Bonferroni post-hoc test: **significant difference from control ($p<0.01$).

bioRxiv preprint doi: https://doi.org/10.1101/2021.07.14.452325; this version posted July 14, 2021. The copyright holder for this preprint (which was not certified by peer review) is the author/funder, who has granted bioRxiv a license to display the preprint in perpetuity. It is made available under aCC-BY-NC 4.0 International license.

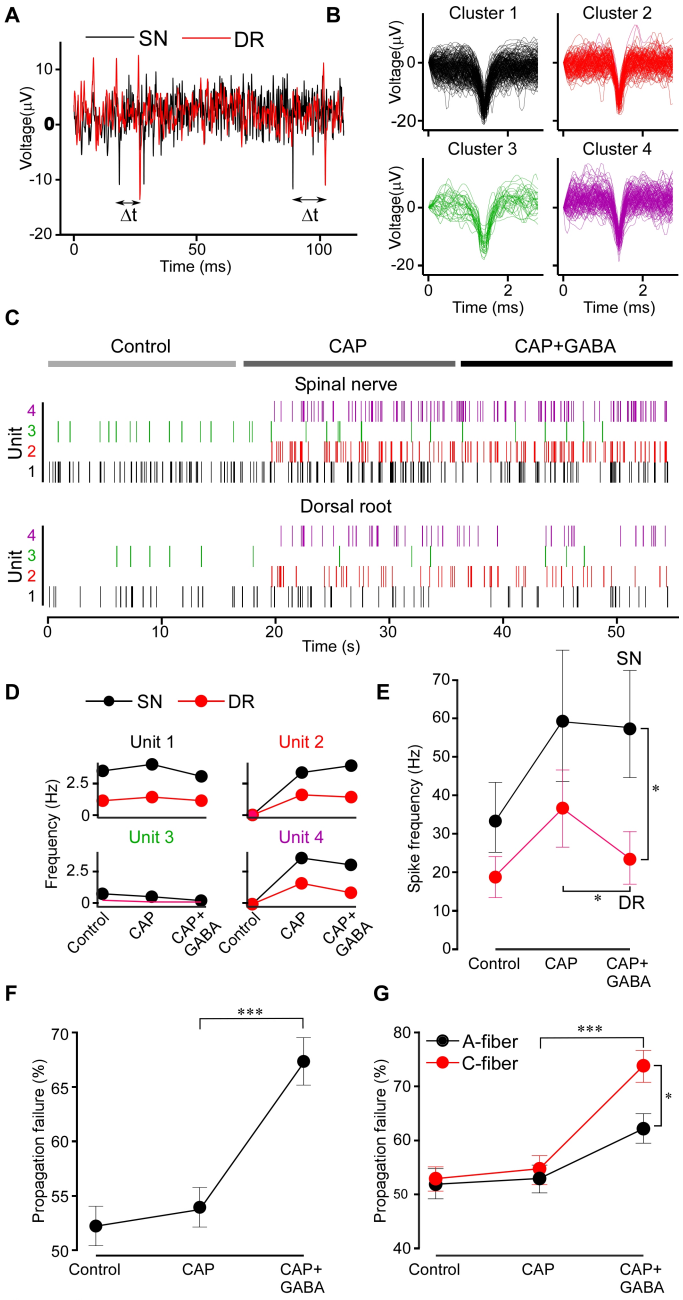

Figure 2

bioRxiv preprint doi: https://doi.org/10.1101/2021.07.14.452325; this version posted July 14, 2021. The copyright holder for this preprint (which was not certified by peer review) is the author/funder, who has granted bioRxiv a license to display the preprint in perpetuity. It is made available under aCC-BY-NC 4.0 International license.

Figure 2. Spike analysis confirms GABAergic filtering. (**A**) Latencies between the SN and DR spikes were measured; the minimum latency defined the SN origin of a DR spike. (**B**) Extracellular spike waveforms extracted from a spinal nerve recording and clustered using WaveClus. (**C**) Raster plot for each clustered waveform (denoted as Unit) under control, CAP and CAP+GABA conditions after matching the DR spikes with these in the SN. Note: capsaicin induced firing of specific units. (**D**) Firing rates of individual units identifies capsaicin-sensitive units. (**E**) Firing rates (matched spikes only) in SN and DR under control, CAP and CAP+GABA conditions. Two-factor (nerve site, drug application) repeated measures ANOVA: main effects associated with drug application [$F(2,10)=6.38$; $p<0.05$], significant interaction between factors [$F(2,10)=10.74$; $p<0.01$]. Bonferroni post-hoc test: *significant difference from control ($p<0.05$). (**F**) Propagation failure (%) of all matched spike units under control, CAP and CAP+GABA conditions. One-way ANOVA: [$F(2,117)=17.7$; $p<0.001$]; Tukey post-hoc test: ***significant difference from CAP, $p<0.001$. (**G**) Units were divided into 'C-type' and 'A-type' based on the SN-DR latency (C: <1.2 m/s; A: >1.2 m/s) and propagation failure rate analyzed as in (F). Two-factor (fiber type, drug application) mixed-effects ANOVA: main effect associated with drug application [$F(2,70)=34.82$, $p<0.001$], significant interaction between factors [$F(2,72)=4.712$, $p<0.05$]. Sidak post-hoc test: *significant difference between CAP+GABA and CAP, significant difference between A and C fibers ($p<0.05$).

bioRxiv preprint doi: https://doi.org/10.1101/2021.07.14.452325; this version posted July 14, 2021. The copyright holder for this preprint (which was not certified by peer review) is the author/funder, who has granted bioRxiv a license to display the preprint in perpetuity. It is made available under aCC-BY-NC 4.0 International license.

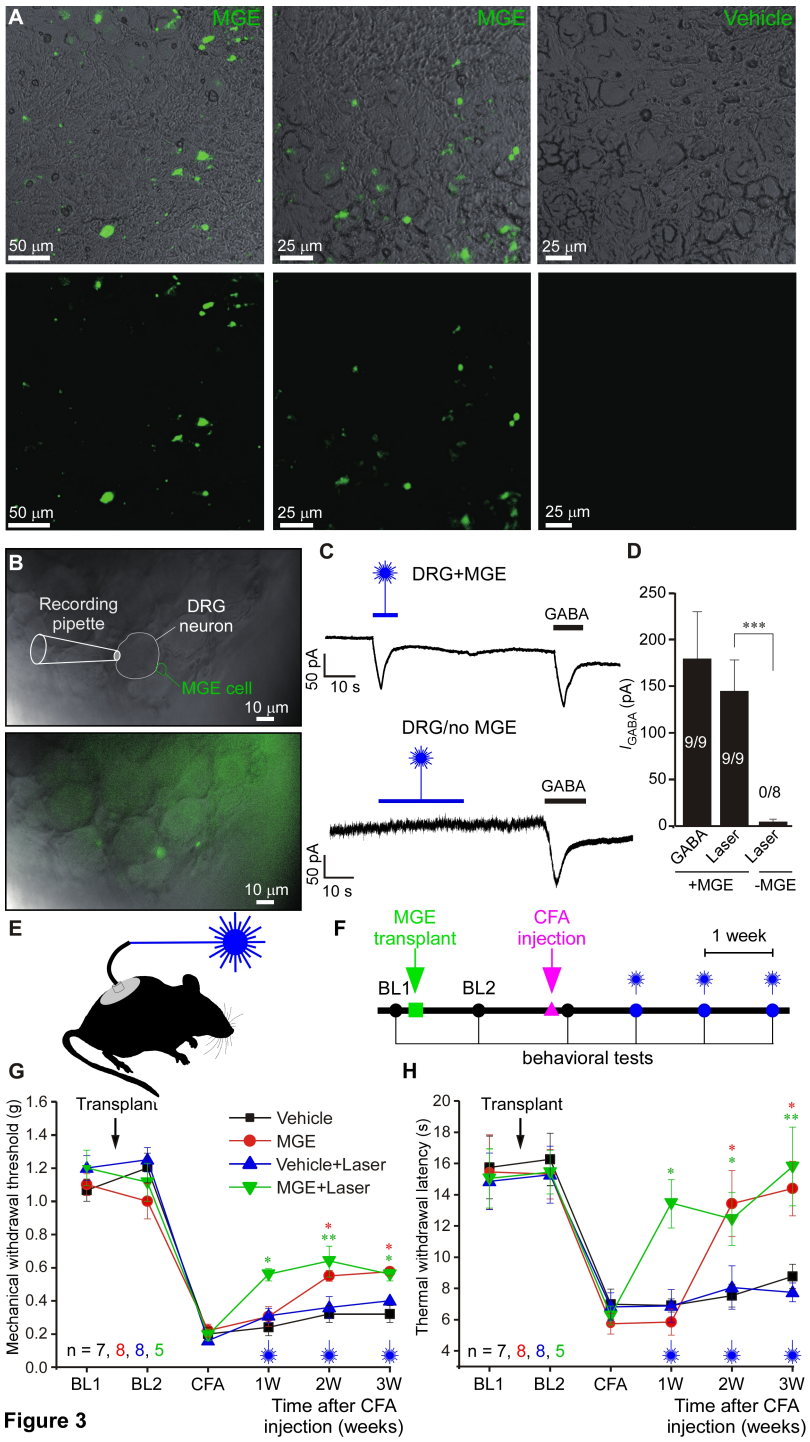

Figure 3

bioRxiv preprint doi: https://doi.org/10.1101/2021.07.14.452325; this version posted July 14, 2021. The copyright holder for this preprint (which was not certified by peer review) is the author/funder, who has granted bioRxiv a license to display the preprint in perpetuity. It is made available under aCC-BY-NC 4.0 International license.

Figure 3. Transplantation of forebrain GABAergic neuron progenitor cells into the adult mouse DRG *in vivo* delivers an analgesic mechanism. (**A**) Fluorescence micrographs of DRG sections of mice DRG 4 weeks after the injection with a suspension of medial embryonic eminence (MGE) cells derived fromVGAT-ChR2-eYFP mice. Control mice (right images) received vehicle injections. (**B**) Bright-field and overlaid fluorescence images of 'loosened' DRG preparation used for patch clamp recording. The whole L4 DRG transplanted with VGAT-ChR2-eYFP MGE cells mice was extracted 4 weeks after transplantation. Recording was made from a DRG neuron juxtaposed to fluorescent MGE cell (top image) using whole-cell voltage clamp. (**C**) Top: example trace of continuous current recording (-60 mV) from the cell shown in B; stimulation with 473 nm blue laser (3 mV) induced inward current, similar in amplitude and kinetics to the current induced by perfusion of GABA (200 μM). Bottom: similar recording from a DRG of a vehicle-injected mice. (**D**) Summary for panel C; one-way ANOVA: $F(2,6)=5.9$; $p<0.01$; Bonferroni post-hoc test: ***significant difference between +MGE vs. -MGE ($p<0.001$). (**E**) Schematic of the *in vivo* optogenetic DRG stimulation. (**F**) Timeline of the *in vivo* behavioral testing after the MGE cell transplantation and hindpaw injection of CFA. (**G**, **H**) Mechanical (G) and thermal (H) hyperalgesia caused by hindpaw injection of CFA 2 weeks after MGE cells transplantation into L4 DRG of mice. At a time of MGE transplantation, mice were also implanted with the fiberoptic light guide. Mechanical and thermal sensitivity was measured using the von Frey and Hargreaves methods, respectively. Starting at one week after the CFA injection measurements were performed while stimulating the L4 DRG with 473nm laser. Black and blue symbols denote control mice DRG-injected with vehicle without and with optogenetic stimulation, respectively. Red and green symbols denote MGE-transplanted mice without and with optogenetic stimulation, respectively. BL1: baseline before transplantation; BL2: baseline after transplantation; CFA: 1 day after the plantar injection of CFA. **G**, Three-factor (MGE vs vehicle, time after CFA, laser stimulation) ANOVA: main effects associated with MGE transplantation [$F(1,4)=50.9$; $p<0.001$], time after CFA [$F(2,3)=6.6$; $p<0.01$]; laser stimulation [$F(1,4)=8.9$; $p<0.01$]. Bonferroni post-hoc test: red* indicate the difference between MGE group and vehicle group within the corresponding time point; green* indicate the difference between MGE with laser stimulation group and vehicle with laser stimulation group; *$p<0.05$, **$p<0.01$. **H**, Three-factor (MGE vs vehicle, time after CFA, laser stimulation) repeated measures ANOVA: main effects associated with MGE transplantation [$F(1,4)=37.4$; $p<0.001$], time after CFA [$F(2,3)=6.1$; $p<0.01$]. Bonferroni post-hoc test: red* indicate the difference between MGE group and vehicle group within the corresponding time point; green* indicate the difference between MGE with laser stimulation group and vehicle with laser stimulation group; *$p<0.05$, **$p<0.01$.

bioRxiv preprint doi: https://doi.org/10.1101/2021.07.14.452325; this version posted July 14, 2021. The copyright holder for this preprint (which was not certified by peer review) is the author/funder, who has granted bioRxiv a license to display the preprint in perpetuity. It is made available under aCC-BY-NC 4.0 International license.

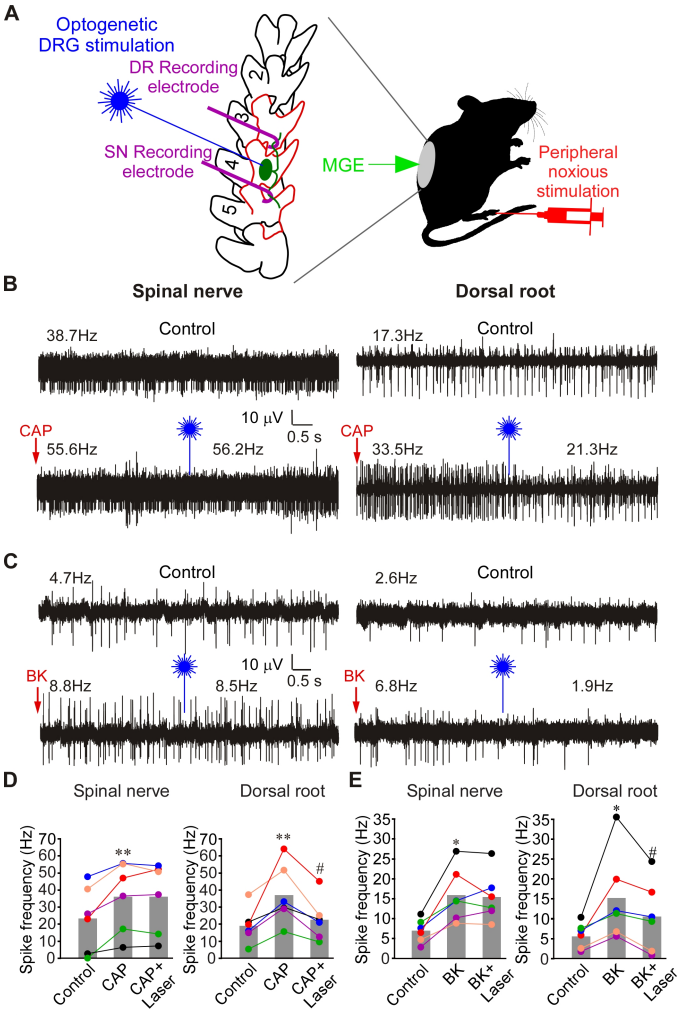

Figure 4

bioRxiv preprint doi: https://doi.org/10.1101/2021.07.14.452325; this version posted July 14, 2021. The copyright holder for this preprint (which was not certified by peer review) is the author/funder, who has granted bioRxiv a license to display the preprint in perpetuity. It is made available under aCC-BY-NC 4.0 International license.

Figure 4. Optogenetic activation of MGE cells in DRG reduces frequency of firing induced by CAP or BK in the DR but not in the SN aspect of the nerve. (**A**) Schematic of the recording paradigm: mice were DRG-transplanted with VGAT-ChR2-eYFP MGE cells 3-4 weeks before recordings; recordings were done as shown in Fig. 1B, supplemented with optical stimulation of the exposed DRG. (**B**) Hindpaw injection of CAP (10 μM, 20 μl) increased firing frequency in both SN and DR branches of the nerve (onset of the bottom traces, as compared to basal activity shown in the upper traces). Application of 473 nm laser light to DRG acutely reduced CAP-induced firing frequency in DR but not SN (bottom traces). (**C**) Experiment similar to A, but BK (100 μM, 20 μl) was hindpaw injected, instead of CAP. (**D**) Summary of panel B. Two-factor (nerve site, drug application) repeated measures ANOVA: main effect associated with drug treatment [$F(2,4)=11.4$; $p<0.05$] and significant interaction between nerve site and treatment [$F(2,4)=7.6$; $p<0.05$]. Bonferroni post-hoc test: **significant difference from control ($p<0.01$); #significant difference from CAP ($p<0.05$). (**E**) Summary of panel C. Two-factor (nerve site, drug application) repeated measures ANOVA: main effect associated with nerve site [$F(1,5)=6.7$; $p<0.05$] and significant interaction between nerve site and treatment [$F(2,4)=9.5$; $p<0.05$]. Bonferroni post-hoc test: *significant difference from control ($p<0.05$); #significant difference from BK ($p<0.05$).

bioRxiv preprint doi: https://doi.org/10.1101/2021.07.14.452325; this version posted July 14, 2021. The copyright holder for this preprint (which was not certified by peer review) is the author/funder, who has granted bioRxiv a license to display the preprint in perpetuity. It is made available under aCC-BY-NC 4.0 International license.

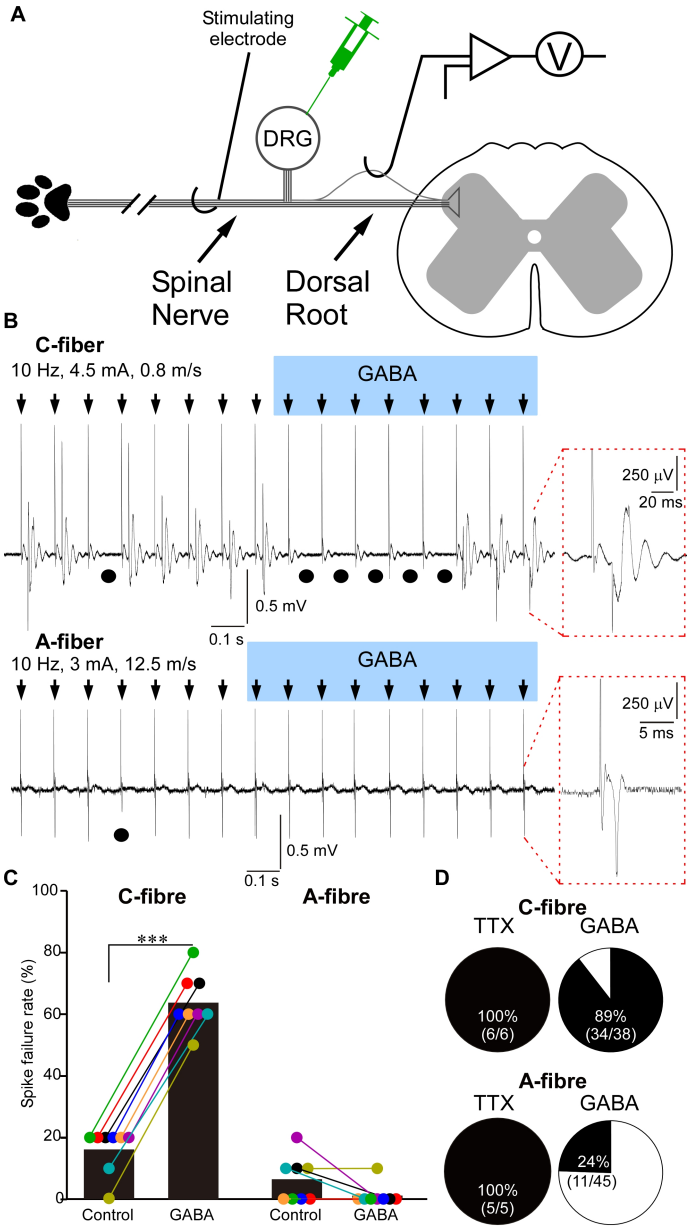

Figure 5

bioRxiv preprint doi: https://doi.org/10.1101/2021.07.14.452325; this version posted July 14, 2021. The copyright holder for this preprint (which was not certified by peer review) is the author/funder, who has granted bioRxiv a license to display the preprint in perpetuity. It is made available under aCC-BY-NC 4.0 International license.

Figure 5. Single-unit recordings: DRG application of GABA induces spike failure at the DRG, which is specific to C fibers. (**A**) Schematic of the single unit recording paradigm. (**B**) Example traces of *in vivo* single unit recording from the DR aspect of a rat C fiber (top) or A fiber (bottom); stimulus electrode is placed in the spinal nerve. Parameters of stimulation and conduction velocity are indicated above the trace. GABA (200 μM, 3 μl) was applied to the DRG during period indicated by blue bar. Stimulus artifacts are indicated by black arrows. Black circles indicate failed spikes. Spike waveform is shown on the extended time scale on the right. (**C**). Spike failure rate before and during application of GABA is analyzed for C and A fibers (8-12 stimulations for each, the control period and during GABA application); n=8 for both fiber types; Two-factor (fiber type, drug application) repeated measures ANOVA: main effect associated with drug application [$F(1,7)=289.0$; $p<0.001$] and significant interaction between fiber type and drug application [$F(1,7)=134.2$; $p<0.001$]. Bonferroni post-hoc test: ***significant difference from control ($p<0.001$). (**D**) Pie charts summarize the percentage of C and A fibers in which TTX or GABA produced a conduction block. Examples of TTX recordings are given in Suppl. Fig. 9. Number of experiments is indicated within each chart.

bioRxiv preprint doi: https://doi.org/10.1101/2021.07.14.452325; this version posted July 14, 2021. The copyright holder for this preprint (which was not certified by peer review) is the author/funder, who has granted bioRxiv a license to display the preprint in perpetuity. It is made available under aCC-BY-NC 4.0 International license.

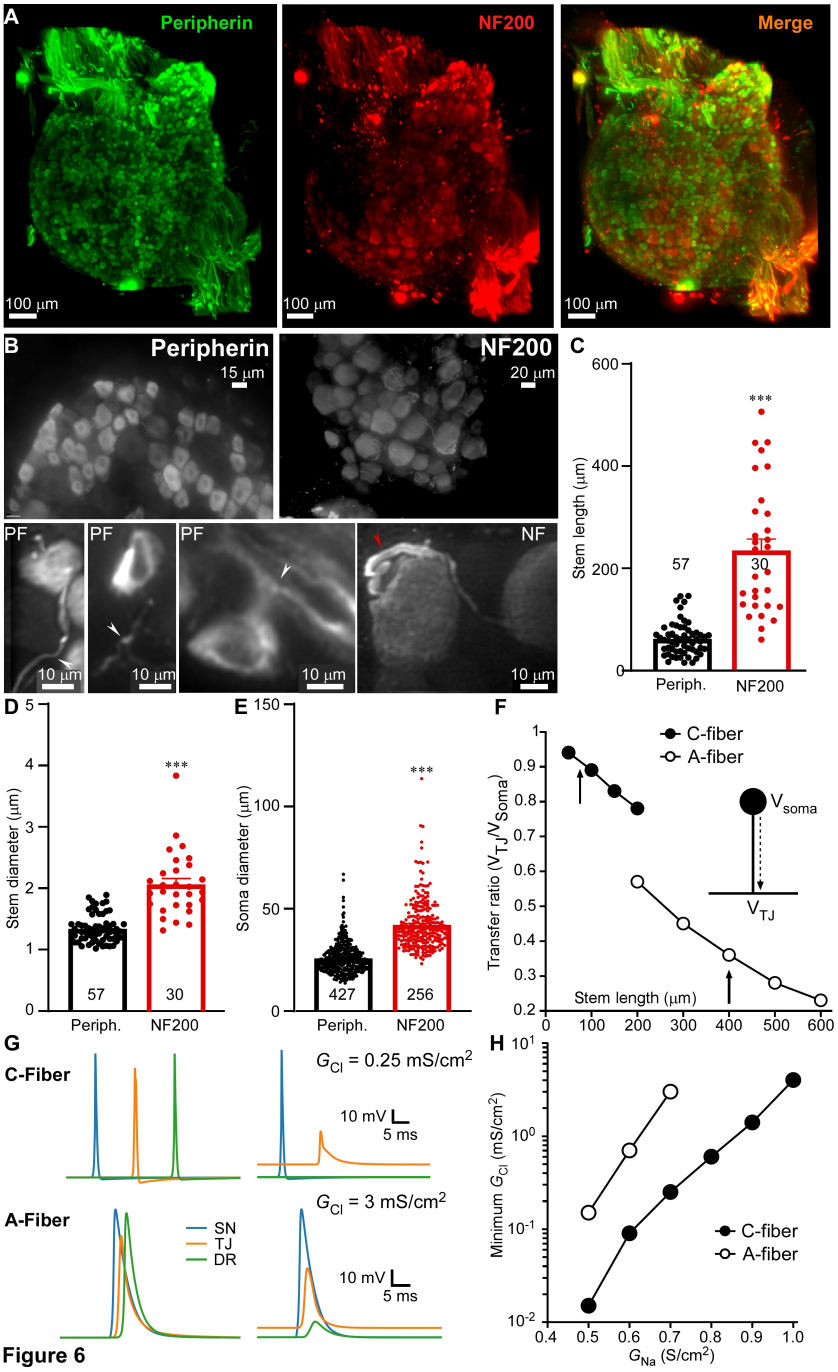

Figure 6

bioRxiv preprint doi: https://doi.org/10.1101/2021.07.14.452325; this version posted July 14, 2021. The copyright holder for this preprint (which was not certified by peer review) is the author/funder, who has granted bioRxiv a license to display the preprint in perpetuity. It is made available under aCC-BY-NC 4.0 International license.

Figure 6. Initial axon morphology defines the efficiency of filtering in DRG. (**A-B**) Light-sheet microscopy of cleared rat DRG (see also Movie S1). C-fibers are labelled with peripherin and A-fibers are labelled with NF-200. Stem axons were traced until bifurcation point using simple neurite tracer in FIJI (Movie S2). White arrowheads indicate t-junctions, red arrowhead point at glomerular region of A-fiber stem axon which increases the length. Quantification of the stem axon lengths (**C**), stem diameter (**D**) and somatic diameter (**E**) of the peripherin- and NF-200-labelled fibers is shown. Data are from 10 lumbar DRGs (peripherin) and 7 lumbar DRGs (NF200) from three rats; n number is given within each bar. Unpaired t-test: $t(85)=9.8$, $p<0.001$ (C); $t(85)=9.8$, $p<0.001$ (D); $t(681)=21.6$, $p<0.001$ (E). Per-animal analysis of data in C-F are shown in Suppl. Fig. 10. (**F-H**) Biophysical model of rat A-type fiber. (**F**) Voltage transfer ratio (potential at the t-junction produced by a potential generated at the soma) as a function of stem length. For A-fibers, this was achieved by varying the number of internode/node pairs. Arrows indicate the typical stem lengths used when simulating spike propagation through the DRG. (**G**) In the absence of somatic G_{Cl} (left traces), spike elicited in the spinal nerve (SN) section of the model propagate through the t-junction (TJ) and into the dorsal root (DR) in both C-fiber and A-fiber models. With a somatic G_{Cl} (right traces), the threshold for blockade in C-fibers is lower. Note that greater G_{Cl} in the A-fiber model produces less depolarization at the soma compared with the C-type model. (**H**) Minimum somatic G_{Cl} for blocking spike propagation is plotted against Na^+ conductance (G_{Na}). For G_{Na} greater than 0.7 mS/cm^2, somatic G_{Cl} was unable to block spike propagation.

bioRxiv preprint doi: https://doi.org/10.1101/2021.07.14.452325; this version posted July 14, 2021. The copyright holder for this preprint (which was not certified by peer review) is the author/funder, who has granted bioRxiv a license to display the preprint in perpetuity. It is made available under aCC-BY-NC 4.0 International license.

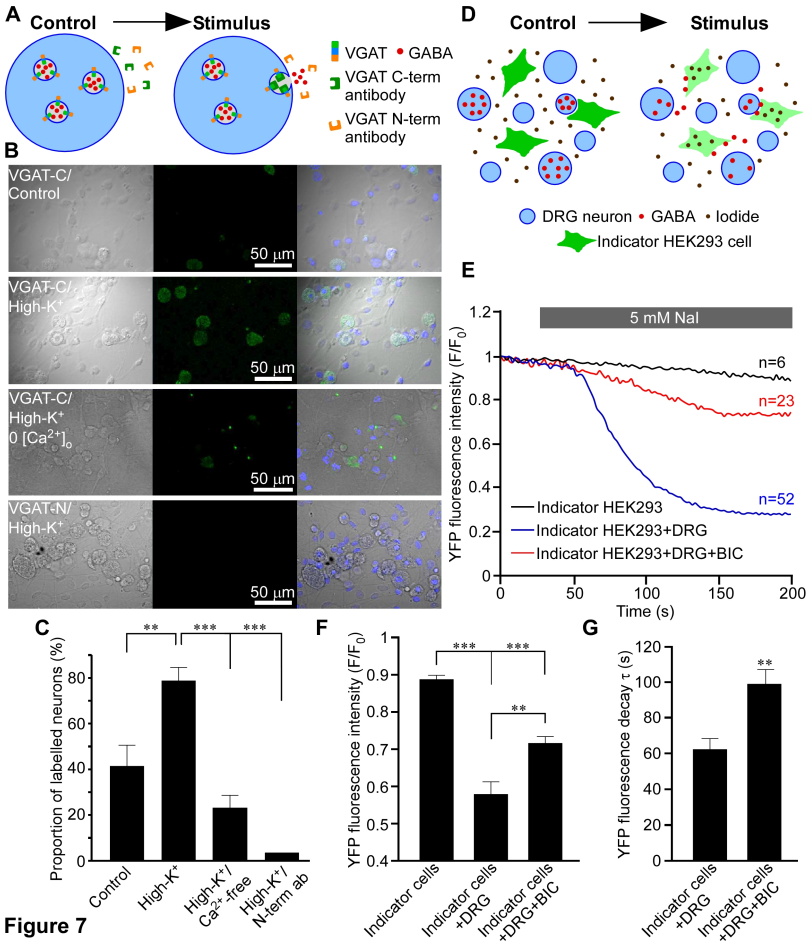

Figure 7

bioRxiv preprint doi: https://doi.org/10.1101/2021.07.14.452325; this version posted July 14, 2021. The copyright holder for this preprint (which was not certified by peer review) is the author/funder, who has granted bioRxiv a license to display the preprint in perpetuity. It is made available under aCC-BY-NC 4.0 International license.

Figure 7. Activity-dependent and spontaneous GABA release of GABA from DRG neurons. (**A-C**) Vesicular GABA release from DRG neurons studied with luminal VGAT antibody uptake. (**A**) Schematic of activity-dependent uptake of luminal (C-terminal) VGAT antibody. (**B**) Bright-field (left), fluorescence (middle) and overlaid images of DRG culture incubated in the presence of either a luminal VGAT antibody (C-term; three upper rows) or a cytoplasmic (N-term; bottom row) antibody. Cells were incubated in the control extracellular solution (upper row) or depolarized by extracellular solution containing 100 mM KCl (second from the top and the bottom rows). In the second from the bottom row Ca^{2+} was excluded from the extracellular solution. (**C**) Summary of experiments like these shown in B (N=3-5, number of neurons is indicated within the columns); quantified is the percentage of stained neurons **p<0.01, ***p<0.01 (Fisher's exact test with Bonferroni correction). (**D-G**) GABA release from DRG investigated with the use of indicator HEK293 cells. (**A**) Schematic of the experiment: HEK293 cells transfected with α1, β2 and γ2 subunits of $GABA_A$ receptors and a halide-sensitive EYFP mutant (H148Q/I152L; EYFP-QL) are co-cultured with DRG neurons and imaged in the presence of 5 mM extracellular iodide. When GABA is present in the extracellular solution, $GABA_A$ channel opening causes I^- influx and EYFP-QL fluorescence quenching. (**E**) Application of NaI induced bicuculline-sensitive EYFP-QL quenching only when indicator HEK293 cells are co-cultured with DRG but not in monoculture; representative traces are shown for each experimental condition. (**F**) Summary for panel E; normalized fluorescence intensity is quantified at 200 s of each recording. Kruskal-Wallis ANOVA: H(2)=33.6, p<0.001; Mann-Whitney post-hoc test: significant difference between indicated groups, **p<0.01, ***p<0.001 (**G**) Quantification of the kinetics of the EYFP-QL fluorescence quenching in experiments shown in E; individual recordings were fit with exponential function and time constants (τ) of the fluorescence decay were analyzed. Mann-Whitney test: U=786, p<0.01. In E-F, data from three independent experiments for each condition are shown, number of cells analyzed is indicated above each trace in panel E.